2019-12-11

Impact of Th1 CD4 TFH skewing on Antibody Responses to an HIV-1 Vaccine in Rhesus Macaques

Anil Verma
University of California, Davis

Et al.

JVI Accepted Manuscript Posted Online 11 December 2019
J. Virol. doi:10.1128/JVI.01737-19

Impact of T_h1 CD4 T_{FH} skewing on Antibody Responses to an HIV-1 Vaccine in Rhesus Macaques

Anil Verma[1*], Brian A. Schmidt[1*], Sonny R. Elizaldi[1, 2], Nancy K. Nguyen[1], Korey A. Walter[3], Zoltan Beck[4,5], Hung V. Trinh[4,5], Ashok R. Dinsarapu[6], Yashavanth Shaan Lakshmanappa[1], Niharika N. Rane[1], Gary R. Matyas[5], Mangala Rao[5], Xiaoying Shen[7], Georgia D. Tomaras[7,8,9,10],Celia C. LaBranche[7], Keith A. Reimann[11], David H. Foehl[11], Johannes S. Gach[12], Donald N. Forthal[12,13], Pamela A. Kozlowski[3], Rama R. Amara[14,15], and Smita S. Iyer[1,16,17#]

[1]Center for Comparative Medicine; [2] Graduate Group in Immunology, UC Davis, CA; [3]Department of Microbiology, Immunology, and Parasitology, Louisiana State University Health Sciences Center, New Orleans, LA; [4]Henry M Jackson Foundation for the Advancement of Military Medicine, Bethesda, MD; [5]US Military HIV Research Program, Laboratory of Adjuvant and Antigen Research, US Military HIV Research Program, Walter Reed Army Institute of Research, Silver Spring, MD; [6]Emory Department of Human Genetics, Emory University, Atlanta, GA; [7]Duke Human Vaccine Institute, Duke University Medical Center, Durham, NC; Departments of [8]Surgery, [9]Medicine,[10]Molecular Genetics and Microbiology, and Immunology, Duke University Medical Center, Durham, NC; [11]Nonhuman Primate Reagent Resource, MassBiologics, University of Massachusetts Medical School, Boston, MA;[12]Division of Infectious Diseases, Department of Medicine, [13]Department of Molecular Biology and Biochemistry, University of California, Irvine School of Medicine, UC Irvine, CA; [14]Department of Microbiology and Immunology, Emory University, Atlanta, GA, [15] Yerkes National Primate Research Center, Emory University, Atlanta, GA; [16]California National Primate Research Center, [17] Department of Pathology, Microbiology, and Immunology, School of Veterinary Medicine, UC Davis, CA

* Both authors contributed equally to this work

[#]Corresponding author
Smita S. Iyer, Ph.D.
Center for Comparative Medicine, Room 2005
County Rd 98 & Hutchinson Drive
Davis, CA 95616
Ph: 530-752-4376
Fax: 530-752-7914
Email: smiyer@ucdavis.edu

Running title: Adjuvants impact Env-specific T_{fh} responses

Word count:

Abstract: 249

Text: 8,112

ABSTRACT

Generating durable humoral immunity through vaccination depends upon effective interaction of follicular helper T cells (T_{fh}) with germinal center (GC) B cells. T_h1 polarization of T_{fh} cells is an important process shaping the success of T_{fh}-GC B cell interactions by influencing co-stimulatory and cytokine-dependent T_{fh} help to B cells. However, the question remains whether adjuvant-dependent modulation of T_{fh} cells enhances HIV-1 vaccine-induced anti-Envelope (Env) antibody responses. We investigated whether an HIV-1 vaccine platform designed to increase the number of T_h1-polarized T_{fh} cells enhances the magnitude and quality of anti-Env antibodies. Utilizing a novel interferon-induced protein (IP)-10-adjuvanted HIV-1 DNA prime, followed by an MPLA+QS-21-adjuvanted Env protein boost in macaques ($D_{IP\text{-}10}$ P_{ALFQ}), we observed higher anti-Env serum IgG titers with greater cross-clade reactivity, specificity to V1V2, and effector functions when compared to macaques primed with DNA lacking IP-10 and boosted with MPLA+alum-adjuvanted Env protein (DP_{ALFA}) The $D_{IP\text{-}10}$ P_{ALFQ} vaccine regimen elicited higher anti-Env IgG1 and lower IgG4 antibodies in serum, showing for the first time that adjuvants can dramatically impact the IgG subclass profile in macaques. The $D_{IP\text{-}10}$ P_{ALFQ} regimen also increased vaginal and rectal IgA antibodies to a greater extent. Within lymph nodes, we observed augmented GC B cell responses and promotion of T_h1 gene expression profiles in GC T_{fh} cells. The frequency of GC T_{fh} cells correlated with both the magnitude and avidity of anti-Env serum IgG. Together, these data suggest that adjuvant-induced stimulation of T_h1-T_{fh} cells is an effective strategy for enhancing the magnitude and quality of anti-Env antibody response.

IMPORTANCE

The results of the RV144 trial demonstrated that vaccination could prevent HIV transmission in humans and that longevity of anti-Env antibodies may be key to this protection. Efforts to improve upon the prime-boost vaccine regimen used in RV144 have indicated that booster immunizations increase serum anti-Env antibody titers but only transiently. Poor antibody durability hampers efforts to develop an effective HIV-1 vaccine. This study was designed to identify the specific elements involved in the immunological mechanism necessary to produce robust HIV-1 specific antibodies in rhesus macaques. By clearly defining immune-mediated pathways that improve the magnitude and functionality of the anti-HIV-1 antibody response, we will have the foundation necessary for rational development of an HIV-1 vaccine.

INTRODUCTION

CD4 T follicular helper cells (T_{fh}) are a specialized subset of CD4 T cells that migrate to germinal centers (GC) within secondary lymphoid organs and provide growth and differentiation signals to GC B cells within a few days of immunization(1-3). GCs are populated by antigen-activated, rapidly proliferating B cell clones, which rely on cytokines and co-stimulatory signals from T_{fh} cells to undergo immunoglobulin affinity maturation, class-switch recombination, and differentiation to memory B cells and plasma cells(4-6). The maturation of GC B cells to plasma cells and the resulting long-lived humoral immunity hinges on effective T_{fh} help.

T_{fh} cells are heterogeneous and, depending on inflammatory signals during T cell priming, differentiate into T_h1, T_h2, T_h17-type T_{fh} cells(7, 8). T_h polarization of a T_{fh} cell influences cytokine profile and co-stimulatory molecule expression, and several recent studies demonstrate that within a single vaccine modality the relative proportion of $T_{fh}1$, -2, or -17 subsets induced following antigen stimulation can influence the duration and functional quality of the antibody response(9). In the setting of influenza and HIV-1 vaccination/infection, the frequencies of vaccine-induced T_h1-polarized, CXCR3-expressing T_{fh} cells correlates with improved antibody titers and enhanced antibody function following immunization(10-12). These data led us to postulate that by stimulating production of T_h1-T_{fh} cells via a tailored vaccine platform, humoral immunity against HIV-1 can be optimized in both duration and quality.

The RV144 trial found that waning serum anti-HIV-1 envelope (Env) IgG titers following vaccination corresponded to a decrease in vaccine efficacy(13, 14). Therefore, there is a critical need to identify strategies that will augment vaccine-mediated humoral immunity for a successful HIV-1 vaccine. In RV144, development of antigen-specific CD4 T cells expressing IL-4 and CD40L, both important in effective T_{fh} help for B cells(15, 16), positively correlated with anti-HIV-1 Env antibody titers. Furthermore, an increase in production of HIV-specific CD4 T cells expressing IL-21, a T_{fh} cytokine that regulates plasma cell differentiation, was also observed(17-19). These data underscore the importance of CD4 T_{fh} cells in HIV-1 vaccine-induced antibody response and suggest that identifying and targeting the optimal T_{fh} subset may be an effective strategy to improve the magnitude and longevity of anti-HIV-1 Env-specific antibodies.

Based on evidence that T_h1-polarized T_{fh} cells correlate with higher antibody responses, we set out to investigate empirically whether an HIV-1 vaccine platform designed to increase the number of T_h1-polarized T_{fh} cells would enhance the functional quality and magnitude of HIV-1 anti-Env antibodies.

Utilizing a novel interferon-induced protein (IP)-10-adjuvanted HIV-1 DNA prime, followed by an MPLA+QS-21-adjuvanted Env protein boost in macaques (D_{IP-10} P_{ALFQ}), we show increased HIV-1 anti-Env specific binding antibody in serum and mucosal compartments compared to vaccination with DNA lacking IP-10 and an MPLA+alum-adjuvanted Env protein boost (DP_{ALFA}). The D_{IP-10} P_{ALFQ} vaccine regimen augmented GC B cell responses and promoted T_h1 gene expression profiles in GC T_{fh} cells. The number of GC T_{fh} cells positively correlated with both magnitude and avidity of anti-Env specific antibody responses. We report for the first time that adjuvants dramatically impact IgG antibody subclass profile in rhesus macaques. We made the striking observation that while both vaccine regimens induced IgG1 antibodies to gp120, the DP_{ALFA} regimen generated much greater IgG4 responses. Together, these data show that by stimulating production of T_h1-T_{fh} cells during the prime and boost using an adjuvanted vaccine, we can enhance the magnitude and function of the anti-HIV-1 -Env antibody response.

RESULTS

Vaccination regimen. Twenty female rhesus macaques were assigned to one of two experimental groups: For Group 1 (n = 10), the D_{IP-10} P_{ALFQ} vaccine group, the T_h1 chemokine, interferon-induced protein (IP)-10, a ligand for and an inducer of CXCR3, was used as a molecular adjuvant to a DNA vaccine, (D_{IP-10}) to prime T_h1-type T_{fh} cells. Group 2 (n=10) animals received the same DNA vaccine without adjuvant (**Figure 1**). The DNA plasmid expressed SIVmac239 Gag, protease, reverse transcriptase, Tat, Rev, HIV C. 1086 Env, and the D_{IP-10} plasmid additionally expressed rhesus IP-10. The DNA was delivered intradermally (ID) with electroporation (EP) in both experimental groups.

Prior to immunizing animals, we evaluated plasmid constructs using 293 T cells. At 48 h following transfection, cells were harvested and expression of HIV proteins was assessed by flow cytometry using the monoclonal antibodies PG9, PG16, PGT121 for surface Env; 2F12 for intracellular SIV Gag, and J034D6 for intracellular IP-10. As illustrated in **Figure 1A** flow plots, both constructs expressed comparable levels of Env and Gag proteins as determined by staining with PGT121 and 2F12, respectively. Cellular and secreted IP-10 as determined by intracellular cytokine staining (**Figure 1A**) and ELISA (**Figure 1C**), respectively, was specific to the DNA IP-10 construct. When expressed as a percent of Gag+ cells, expression of trimeric Env as determined by binding of the monoclonal broadly neutralizing antibodies PG9, PG16 that bind the V1 V2 loop and the V3 binding monoclonal PGT 121 showed comparable expression across the two vaccine constructs.

Following DNA immunization, we used clade C C.ZA 1197MB gp140 protein adjuvanted with Army Liposome Formulation (ALF) liposomes containing monophosphoryl lipid A (MPLA) and a detoxified saponin derivative, QS-21 (ALFQ)(20) to boost T_h1 primed responses (**D_{IP-10} P_{ALFQ}**) (**Figure 1D**). Group 2 animals received an unadjuvanted ID, EP delivered DNA prime and protein adjuvanted with aluminum-adsorbed ALF formulation (ALFA) (21), wherein the protein was adsorbed to aluminum hydroxide and then added to ALF (**DP_{ALFA}**). Blood was collected at weeks -8 and 0 of vaccination, and at weeks 1, 2, 4, 8, 18, and 20 following each vaccination, as indicated. Fine needle aspirates of lymph nodes (LN) or LN biopsies (draining) were collected to examine GC responses, and rectal and vaginal secretions were sampled to assess mucosal antibodies.

To confirm that the D_{IP-10} P_{ALFQ} vaccine regimen induced relatively higher T_h1-biased inflammatory responses, we evaluated induction of CXCR3 ligands in serum using a flow-based Legend plex assay at days 0, 3, and 7 after the 1st protein boost. The data showed higher relative induction of IP-10 and the interferon-inducible T cell alpha chemoattractant (I-TAC) in the ALFQ-adjuvanted animals ($p < 0.01$, **Figure 1E**). Monokine induced by gamma, another CXCR3 ligand, was not induced following the 1st protein boost in either vaccine regimen (data not shown). We also observed significant induction of IL-6 following the ALFQ protein boost. Induction of the chemokine regulated upon activation, normal T cell expressed, and secreted (RANTES) in both vaccine groups indicated presence of activated CD4 and CD8 T cells following vaccination. In all, these data showed higher relative magnitude of T_h1 chemokines in the D_{IP-10} P_{ALFQ} vaccine regimen.

D_{IP-10} $Protein_{ALFQ}$ vaccine induces robust and durable anti-Env antibody titers with cross-clade breadth. To ascertain whether induction of greater magnitude T_h1 inflammatory responses elicited anti-Env antibody responses of different magnitudes between the vaccine regimens, we first evaluated responses against C.1086 gp140 Env using a binding antibody multiplex assay (BAMA)(22). We have previously shown that the transient extrafollicular plasmablast response contributes to peak serum IgG antibody titers following the boost, while titers at week 8 and beyond are mainly plasma cell derived(12). Therefore, we assessed antibody levels at weeks 0, 2, and 8 following each of the protein boosts to capture both extrafollicular (week 2) and plasma cell-derived (week 8 and beyond) titers. The data showed robust induction of anti-C.1086 Env responses following the 1st protein immunization in all 20 animals and potent recall of memory B cells following the 2nd protein immunization as evidenced by a robust boost in antibody responses (**Figure 2A**). Strikingly, Env ALFQ boosted animals developed significantly higher responses against C.1086 gp140; median AUC values in ALFA and ALFQ vaccine groups were: wk 0, 7496 and 20301, $p < 0.01$; wk 2, 46481 and 63469, $p < 0.001$; wk 8, 20714 and 36709, $p < 0.0001$ post 2nd protein boost.

We confirmed these findings by using an independent ELISA assay to explore C.1086 gp140 anti-Env antibody kinetics after the 2nd protein boost (**Figure 2B**). The assay revealed that anti-Env titers exhibited a median 5-

245 fold increase at week 2 post-2nd protein immunization relative to week 0 indicating a successful booster
246 response. In affirmation of the BAMA data, antibody titers were significantly higher in the D_{IP-10} P_{ALFQ}
247 group compared to the DP_{ALFA} group at all time points post the 2nd protein boost.
248
249 We next assessed the breadth of the serum IgG antibody response and found that AUC values against CH505
250 subtype C Env were also significantly higher in the D_{IP-10} P_{ALFQ} group relative to the DP_{ALFA} group ($p< 0.01$,
251 **Figure 2C**). Similarly, increased responses against the Con S (group M consensus) and Con C proteins at
252 week 2 following the 2nd protein boost in the D_{IP-10} P_{ALFQ} group were sustained at week 8 demonstrating greater
253 induction of antibodies with cross-clade breadth using the D_{IP-10} P_{ALFQ} vaccine regimen ($p< 0.05$, **Figure 2D,E**).
254 We also assessed binding to gp120 V1V2 loops from isolate Case A2, scaffolded on murine leukemia virus
255 (MLV) gp70, at weeks 2 and 8 and found that significantly higher specificity to these important regions was
256 induced by the D_{IP-10} P_{ALFQ} vaccine regimen following the second protein boost ($p < 0.05$, **Figure 2F**).
257
258 Based on significantly elevated anti-Env antibody responses in the D_{IP-10} P_{ALFQ} vaccine regimen we sought to
259 quantify decline in antibody magnitude. To this end, we calculated fold change in titers at week 8 and 18
260 following 2nd protein boost relative to titers at week 8 post 1st protein boost. Significantly higher titers at week 8
261 (mean 1.7-fold in DP_{ALFA} versus 4.5-fold in D_{IP-10} P_{ALFQ} group; $p< 0.05$) and week 18 (mean 0.3-fold in DP_{ALFA}
262 versus 1.3-fold in D_{IP-10} P_{ALFQ} group; $p< 0.01$) post 2nd protein boost in D_{IP-10} P_{ALFQ} vaccinated animals
263 suggested that the D_{IP-10} P_{ALFQ} vaccine regimen was effective at enhancing magnitude of anti-HIV-1 Env serum
264 IgG titers (**Figure 2G**). Together, the data show that the D_{IP-10} P_{ALFQ} group had higher induction of cross-clade
265 breadth, elicited stronger binding to a gp70-V1V2 protein, and enhanced antibody responses relative to the
266 DP_{ALFA} group.
267
268 **D_{IP-10} $Protein_{ALFQ}$ vaccine elicits high avidity anti-Env antibody with ADCC and ADP activities.** Next, we
269 quantified avidity of IgG binding antibodies (as disassociation constants, kd) in sera collected at 2 weeks post
270 final DNA prime and after each of the protein boosts using Surface Plasmon Resonance (SPR) to C.1086
271 gp140 protein (23). The data showed that gp140-specific antibodies reached higher avidity with each
272 sequential immunization in both vaccine groups ($p < 0.0001$, **Figure 3A, B**). Consistent with ELISA results

(**Figure 2**), SPR-based IgG measurements, expressed as relative units, showed significantly higher gp140 IgG in the D_{IP-10} P_{ALFQ} vaccine group ($p < 0.0001$, **Figure 3C)**. Therefore, we normalized avidity measurements to gp140 binding measurements and observed increased avidities in the D_{IP-10} P_{ALFQ} vaccine group relative to the DP_{ALFA} group, which was suggestive of more productive GC reaction in the D_{IP-10} P_{ALFQ} vaccine group ($p < 0.0001$, **Figure 3C**). To confirm that higher avidity antibodies in the D_{IP-10} P_{ALFQ} vaccine group were sustained, we determined avidity at 8 weeks following the 2nd protein boost using a 2M sodium thiocyanate displacement ELISA with C.1086C gp140 antigen(12). The data showed sustained induction of higher avidity antibodies in the D_{IP-10} P_{ALFQ} group ($p < 0.05$, **Figure 3D**), which was further corroborated with a 0.1 M sodium citrate ELISA ($p < 0.01$, **Figure 3E**). Notably, higher avidity antibodies against Con C and Con S gp140 proteins were also induced in the D_{IP-10} P_{ALFQ} vaccine regimen ($p < 0.01$, **Figure 3F,G**).

After establishing induction of higher avidity antibodies in the D_{IP-10} P_{ALFQ} vaccine group, we next evaluated capacity of immune sera to neutralize HIV-1 using the classic TZM-bl assay(12). We detected robust activity against MW965.26, a subtype C tier 1A variant (**Figure 3H**) whereas neutralization of tier 1B and tier 2 isolates was sporadic (data not shown)(24). The data showed higher induction of tier 1A neutralizing antibodies in the D_{IP-10} P_{ALFQ} vaccine group (ID50 range at week 2 post 2nd protein boost DP_{ALFA}: 37 -1126; D_{IP-10} P_{ALFQ}: 195-4977, $p < 0.01$). These titers dropped to an ID50 value of 20 in the DP_{ALFA} group but were maintained between 24-1057 in the D_{IP-10} P_{ALFQ} group ($p < 0.001$). To assess generation of Fc-mediated antibody effector responses, we measured antibody-dependent cellular cytotoxicity (ADCC) and antibody-dependent phagocytosis (ADP) triggered by engagement of the Fc receptors on antibody-bound target cells by innate cells (25) (26, 27). ADCC was assessed by measuring killing of Clade C CH505 SHIV-infected CEM.NKR target cells by a rhesus CD16+ (FcγR3) NK cell line in the presence of immune serum. As shown in **Figure 3I,** serum from D_{IP-10} P_{ALFQ} vaccinated animals demonstrated significantly greater ADCC activity at week 2 and week 8 after the 2nd protein boost when compared to DP_{ALFA} immunized animals ($p < 0.01$). Serum collected from D_{IP-10} P_{ALFQ} vaccinated animals at week 8 post protein boost 2 also mediated significantly greater phagocytosis of C.1086 gp120-coated beads by the CD32+ (FcγR2) and CD64+ (FcγR1) THP-1 monocytic cell line (**Figure 3J and K).** To determine if the adjuvants given to animals in the vaccine groups generated different rhesus IgG subclass antibody repertoires, we quantified C.1086 gp120-specific IgG1, IgG2, IgG3, and

IgG4 by ELISA. We found that IgG2 and IgG3 antibodies were extremely low and did not differ between groups (**Figure 3L**). However, D_{IP-10} P_{ALFQ} vaccinated animals had higher gp120-specific IgG1 ($p < 0.0001$, **Figure 3L**) while DP_{ALFA} vaccinated animals had higher gp120-specific IgG4 resulting in markedly elevated IgG1/IgG4 ratio in the D_{IP-10} P_{ALFQ} vaccine group ($p < 0.001$, **Figure 3M**). The IgG4 detection antibody (clone 78A) showed minimal cross-reactivity to IgG1 and IgG3 subclass antibodies indicating specificity of the antibody to rhesus IgG4 (data not shown). These results are consistent with the report that antibodies of the IgG1 subclass are the most abundant in rhesus macaques (28, 29).

$DNA_{IP-10}Protein_{ALFQ}$ vaccine elicits robust anti-Env antibody in vaginal and rectal mucosal compartments. Having established induction of higher serum IgG antibody titers in D_{IP-10} P_{ALFQ} vaccinated animals, we next sought to determine whether mucosal anti-Env antibodies were also correspondingly increased. To this end, we assayed rectal and vaginal secretions for C.1086 gp140-specific IgG and IgA antibodies at baseline and longitudinally after each of the protein boosts. We next asked whether either vaccine regimen induced mucosal antibody responses; we focused on quantifying concentrations following the 1st protein boost, a time point when mucosal IgG and IgA concentrations are above baseline (background) levels in the majority of the animals. The appearance of gp140-specific IgG in secretions closely mimicked the kinetics of the serum IgG antibody response, with each protein boost increasing levels of Env-specific IgG antibodies in vaginal and rectal secretions (**Figure 4A and B**). As in serum, the D_{IP-10} P_{ALFQ} vaccine regimen generated higher levels of specific IgG in secretions when compared to the DP_{ALFA} vaccine. The gp140-specific IgA in vaginal and rectal secretions was also increased to a greater extent by the D_{IP-10} P_{ALFQ} vaccine regimen (**Figure 4C and D**). Notably, at week 16-post 2nd protein boost, vaginal IgA antibodies were still above the limit of detection in most D_{IP-10} P_{ALFQ} vaccinated animals but in only 2 of 10 DP_{ALFA} vaccinated animals. Analysis of gp140-specific IgA in serum revealed higher induction in the D_{IP-10} P_{ALFQ} group (**Figure 4E**). However, the kinetics of the serum IgA response in D_{IP-10} P_{ALFQ} as well as DP_{ALFA} animals differed strikingly from the mucosal IgA responses, especially in the reproductive tract (**Figure 4C-D**), suggesting a true mucosal (locally-derived) IgA response was generated in these animals. This was most evident after the 2nd protein boost, when vaginal IgA antibodies to gp140 were found to be dramatically increased but serum IgA antibodies were reduced (**Figure 4A and C**). Together, these data demonstrate that the D_{IP-10} P_{ALFQ} vaccine regimen was more effective

than the DP_{ALFA} regimen for generating higher magnitude Env binding antibodies in serum and secretions, as well as serum IgG antibodies with greater breadth, avidity, and function.

Next, we determined whether the relatively higher antibody concentrations of anti-gp140 antibody in mucosal secretions in the D_{IP-10} P_{ALFQ} vaccine group might result in delayed acquisition against the Clade C transmitted/founder virus, SHIV.C.CH505. To this end, we challenged monkeys intra-vaginally with eight repeat, low-dose inoculations of SHIV.C.CH505 at week 20 post the 2nd protein boost. While we observed no significant differences in delay in acquisition between the vaccine groups, 3 of 10 animals in the D_{IP-10} P_{ALFQ} vaccine group were protected relative to 0 of 10 animals in DP_{ALFA} regimen (**Figure 4F**). We observed that mucosal gp140 IgG antibody concentrations at week 16 post 2nd protein boost was a correlate of protection, with higher concentrations correlating with delayed acquisition in infected animals in each of the vaccine groups ($r = 0.94$, $p < 0.01$; D_{IP-10} P_{ALFQ} vaccine group, $n = 7$; $r = 0.78$, $p < 0.01$; DP_{ALFA} vaccine group, **Figure 4G**).

D_{IP-10} $Protein_{ALFQ}$ vaccine induces Env-specific T_{fh} cells and GC T_{fh} cells with distinctive T_h1 signatures. The D_{IP-10} P_{ALFQ} vaccine promoted anti-Env antibody magnitude and functionality following the 1st protein boost. Based upon this finding, we wanted to determine whether this vaccine regimen also correspondingly enhanced T_{fh} cells in the periphery and LNs. To this end, we first assessed whether higher frequencies of Env-specific T_{fh} cells were induced in blood 7 days after the 1st protein boost, corresponding to the peak of the effector response. PBMCs were stimulated with overlapping peptide pools representing Con C gp140 together with the HIV-1 C.1086 Env gp140C protein C. The induction of the activation markers CD25 and OX40 was assessed by flow cytometry after stimulation (**Figure 5A**, flow plot)(30). The analysis revealed a higher frequency of Env-specific CD4 T cells in the circulation of D_{IP-10} P_{ALFQ} animals. When expressed as a percentage of $CD95^+$ CD4 T cells, median frequencies of Env specific-CD4 T cells were on average 10-fold higher in the D_{IP-10} P_{ALFQ} group indicative of a higher magnitude Env-specific T_{fh} response ($p < 0.001$, **Figure 5B**). In all, these data showed robust recall responses following the 1st protein boost with higher relative magnitude of Env-specific T_{fh} cells in the D_{IP-10} P_{ALFQ} vaccine regimen.

Next, we assessed LN responses using biopsies collected at day 14 post 1st protein boost and identified GC T_{fh} cells as $CXCR5^+$, PD-1^{+++} cells (red population, **Figure 6A**) and GC B cells as Ki-67^+, Bcl-6^+ CD20 cells. As expected, GC T_{fh} cells expressed Bcl-6 and ICOS and consistent with the functional ability of T_{fh} cells (12), our *ex vivo* analysis of sorted GC T_{fh} cells revealed their capacity to support IgG production by autologous LN B cells (**Figure 6B**). Evaluation of GC T_{FH} frequencies over the course of immunization revealed a significant induction of GC T_{fh} cells 2 weeks after protein boost 1 relative to baseline, and significantly higher frequencies 2 weeks after protein boost 2 relative to week 0 of protein boost 2 (**Figure 6C**).

While frequencies of GC T_{FH} cells were not significantly different between experimental groups, we found that GC B cell frequencies were significantly higher in the D_{IP-10} P_{ALFQ} vaccine regimen (n=10 animals in each group following the 1st protein boost; median DP_{ALFA}: 14.2% (of $CD20^+$ cells) versus D_{IP-10} P_{ALFQ} : 25%, $p < 0.05$ and the frequency of GC T_{fh} cells strongly correlated with GC B cell responses (**Figure 6D)**. Importantly, Env-specific T_{fh} cell frequencies in the LN directly correlated with GC T_{fh} cell frequencies but not memory T_{fh} cells indicating that GC T_{fh} cells were enriched for vaccine-induced follicular cells ($p<0.0001$, **Figure 6D**). Next, we assessed expression of CXCR3, which is heterogeneously expressed by GC T_{fh} cells (**Figure 6E**) and found higher expression of CXCR3 on GC T_{fh} cells in the D_{IP-10} P_{ALFQ} group. We observed that the frequency of $CXCR3^+$ T_{fh} cells within the GC was directly associated with gp140 serum antibody titers at week 18 post 2nd protein boost ($r = 0.44$, $p < 0.05$; **Figure 6E**). Examination of GC B cells showed elevated CXCR3 expression in GC B cells from the D_{IP-10} P_{ALFQ} vaccine group ($p< 0.05$, **Figure 6F**). Notably, T-bet expression on B cells, a marker of memory B cells (31), corresponded with CXCR3 expression, suggesting a mechanistic basis for enhanced antibody responses in the D_{IP-10} P_{ALFQ} vaccine group. Together, these data support the contention that T_h1 skewing of CD4 T_{fh} cells may support higher anti-Env antibody.

To gain insights into the molecular mechanisms underlying successful antibody responses we next determined transcriptional signature in GC T_{fh} cells. To achieve this goal, we sorted naive CD4 cells, CD4 Tfh cells, and memory CD4 cells from the LNs of 3 D_{IP-10} P_{ALFQ} group animals with highest gp140 serum IgG at week 8 post 1st protein boost. These subsets were identified using the following markers: naive cells (CD4+CD95-), T_{fh} cells

(CD95+CXCR5+PD-1+/++), memory T_{fh} cells (CD95+CXCR5+ PD-1-), and memory non-T_{fh} cells (CD95+ CXCR5-PD-1-).

RNA samples meeting quality control checks were sequenced using 3'-Tag-RNA-Seq library prep protocol at the UC Davis Genome Center using the Illumina HiSeq 4000 platform. Prior to analysis of sequenced single-end reads, genes with fewer than 40 counts per million reads were filtered, leaving 7,086 genes. Differential expression analyses were conducted using the limma-voom Bioconductor pipeline (32) to compare the transcriptome profiles of antigen-experienced CD4 subsets to naive cells. Principal component analysis of the 500 most variable genes based on coefficient of variation showed that CD4 transcriptomes clustered by cellular differentiation status, with memory CD4 T cells (both CXCR5+ and CXCR5-) sharing transcriptional signatures relative to naive and T_{fh} subsets (**data not shown**). To extract information on biologically relevant gene-sets, we performed gene set enrichment analysis with the goal of determining biological pathways that were enriched in T_{fh} cells in the T_h1 vaccine regimen. Genes regulating interleukin (IL)-12, tumor necrosis factor (TNFa), interferon gamma (IFNG), and IL-6 production were strongly enriched in T_{fh} cells. Consistent with metabolic activity of effector cells and functional capacity of T_{fh} cells, pathways regulating cellular metabolism, glucose homeostasis, and B cell proliferation were also enriched.

To determine transcriptional activity of T_{fh} cells in the D_{IP-10} P_{ALFQ} vaccine group, we focused on differentially induced genes in T_{fh} cells relative to naive cells (n=89, adj. $p < 0.05$, **Figure 6G**), of which induction of key T_{fh} transcripts including CXCR5, ICOS, and Bcl-6 was common to both T_{fh} cells and memory T_{fh} cells. Heatmap shows expression of genes differentially expressed in T_{fh} cells relative to naive across four sorted CD4 subsets. Consistent with representation of D_{IP-10} P_{ALFQ} genes in GSEA, T_{fh} cells showed higher expression of TBX21 and IFNG (**Figure 6G,H**). The class IV semaphorin protein (SEMA4A), a co-stimulatory molecule expressed by D_{IP-10} P_{ALFQ} cells(33) was significantly induced as was high-mobility group box 1 (HMGB1), an inflammatory mediator regulating TNF and IL-6 production (34). Induction of IL-18R suggested the capacity of IL-18 to drive IFNG production within the GC(35). Likewise, we noted higher expression of receptor interacting serine/threonine kinase 2 (RIPK2) which drives IFNG in T_h1 cells and contributes to T_h1 differentiation (36). The corresponding downregulation of IL-4R in T_{fh} cells indicated enrichment of the T_h1 program within T_{fh} cells

409 in D_{IP-10} Pro_{ALFQ} vaccinated animals. This together with increased protein expression of CXCR3 within the GC
410 suggested that CD4 T cell help for humoral immunity was driven by T_h1 T_{fh} cells in the D_{IP-10} P_{ALFQ} vaccine
411 regimen.
412
413 **DNA_{IP-10} immunization induces systemic expansion of pro-inflammatory monocytes and enhances GC**
414 **T_{fh} responses.** Based on increased frequencies of Env-specific T_{fh} cells and evidence for induction of a T_h1
415 transcriptome program in D_{IP-10} P_{ALFQ} vaccinated animals after the 1st protein boost, we sought to assess T_{fh}
416 responses during the DNA priming phase. First, we evaluated blood to quantify activated $CXCR5^+$ CD4 T cells
417 in both vaccine groups **(Figure 7A**). Based on co-expression of ICOS and PD-1, activation markers induced
418 upon TCR stimulation, the data showed that DNA immunization significantly increased the relative frequencies
419 and absolute counts of $ICOS^+$ $PD\text{-}1^+$ $CXCR5^+$ CD4 T cells in blood at day 14 (n=20; median frequencies, day
420 0: 3.38%; day 14: 6.7%, $p < 0.0001$; n =20; absolute counts, day 0: 3.04; day 14, 8.7 day 14, $p < 0.01$, **Figure**
421 **7A**) in both experimental groups indicating that DNA delivery by electroporation was immunogenic.
422
423 Next, we assessed whether DNA immunization elicited humoral responses against SIV Gag and HIV Env
424 proteins expressed in the plasmid. We found that detectable responses to Gag were observed in 45% of
425 animals at week 2 of the 1st DNA prime, in 65% at week 2 following the 2nd DNA prime, and all animals
426 following the 3rd DNA prime (**Figure 7B,** significance symbols compare immunization time points relative to
427 baseline). Antibody responses to C.1086 Env were low and undetectable until the 2nd DNA prime (data not
428 shown), but were observed in majority of animals following DNA3 (**Figure 7C,** significance symbols compare
429 immunization time points relative to baseline). Gag and Env antibody titers were not significantly different
430 between the vaccine regimens during the DNA primes. Based on robust induction of anti-Gag antibody
431 responses, we determined whether Gag specific CD4 T cells were induced at week 1 following DNA3, when
432 the CD4 effector response peaked. PBMCs were stimulated with pooled SIVmac 239 Gag peptide pools and
433 interrogated for expression of activation markers (AIM) and for induction of cytokines (ICS). The AIM assay
434 captured a higher proportion of Gag-specific CD4 T cells (**Figure 7D**) and together, these data indicated that
435 the DNA immunization was sufficiently immunogenic to prime T and B cell responses.
436

Based on the induction of antibody and T cell responses following DNA3, we next assessed whether a concomitant acute induction of pro-inflammatory monocytes (innate cells that drive T_{fh} responses) preceded the appearance of these cells in blood (37, 38). We quantified frequencies of $CD14^+$ $CD16^+$ HLA-DR+ (lineage-) cells in blood (**Figure 7 E,F**) and discovered rapid and robust expansion of pro-inflammatory monocytes in both vaccine groups with significantly higher induction in the D_{IP-10} P_{ALFQ} vaccine group **(Figure 7G**). Based on this, we asked if LN responses differed between vaccine groups. Strikingly, the GC T_{fh} cell frequencies within the fine-needle aspirates of the draining LN were higher in the D_{IP-10} P_{ALFQ} vaccine group following the 3rd DNA immunization (**Figure 7H**). Notably, the greater inflammatory response was associated with increased levels of serum IgG antibodies, linking the innate immune response to priming of effective CD4 T_{fh} help (**Figure 7I)**.

DISCUSSION

The present study gives rise to three main conclusions; first, that an HIV-1 vaccine platform designed to promote T_h1-polarized T_{fh} cells increases the number of circulating Env-specific T_{fh} cells, enhances GC responses, increases anti-Env binding antibody titers in sera, stimulates serum antibody effector functions. Second, that a T_h1 vaccine regimen can elicit anti-Env vaginal and rectal IgA responses; and third that induction of high avidity antibodies, reflective of productive GC responses, are engendered by a T_h1 vaccine regimen. Collectively, the data suggest that adjuvant-induced stimulation of T_h1-T_{fh} cell production during the vaccine prime and boost is an effective strategy to enhance magnitude and functionality of the anti-Env antibody response.

Productive T cell responses critically depend on cytokine signals during priming, and recent studies demonstrate that monocyte-derived cytokines drive effective CD4 T cell differentiation and T_{fh} responses (38-40). Here, investigation of the kinetics of pro-inflammatory monocytes - cellular innate biomarkers of adjuvanticity - revealed a transient increase in $CD14^+CD16^+$ monocytes in blood with a higher relative increase in the D_{IP-10} P_{ALFQ} vaccine group. Strikingly, fine-needle aspirates of the draining LNs showed higher GC frequencies in the D_{IP-10} P_{ALFQ} vaccine group, indicating active/productive GC responses. Notably, the improved inflammatory response was associated with increased antibody magnitude linking the innate immune response to effective induction of CD4 T_{fh} cells. Although titers against Gag and Env were not significantly different between the vaccine regimens during the prime, it is possible that the higher memory B cells, which we did not quantify, were induced with the T_h1 prime. Indeed, several recent studies show that potent priming of the immune response sets the stage for stronger boosting of cellular and humoral immunity in the setting of DNA prime, NYVAC boost and Ad5 prime, NYVAC boost vaccine regimens(25, 41). The effectiveness of priming is not limited to CD4 T cells and B cells; a DNA vaccine targeting conserved elements of SIV Gag robustly primes cytotoxic T cells which are effectively boosted following a long rest period(42, 43). These data open the possibility to a critical window of opportunity during the priming phase. This window can be exploited to prime for long-lasting, durable CD4, CD8 T cell, and antibody responses to HIV-1 vaccination.

The HVTN studies 070 and 080 employed the IL-12 DNA adjuvanted plasmid with the subtype B PENNVAX-B (PV) DNA plasmid and showed 80% response rates after the third DNA vaccination in PV+IL-12 recipients compared to a 44% response rate with the PV alone vaccine. A subsequent follow up study demonstrated robust recall of binding anti-Env antibody titers with ADCC activity following an MVA boost in PV+IL-12 recipients (44, 45). Because IL-12 is a classic innate mediator of T_h1 responses, the data suggest that an increase in T_h1 GC T_{fh} cells may underlie the observed effects. Correspondingly, studies in rhesus macaques with an ALVAC prime, ALVAC + gp120 protein boost using SIV immunogens showed higher SIV Env titers with MF59 compared to aluminum adjuvanted protein boosts 2 weeks following the final immunization(46). While T_{fh} responses and memory antibody titers were not examined, a recent study in humans showed enhanced binding antibody titers 26 weeks after booster immunization with a T_h1 GLA-SE-adjuvanted malaria antigen relative to one formulated in aluminum(47). These studies in conjunction with our report provide support to the immune potential of T_h1-T_{fh} cells in fostering high magnitude antibody titers. In contrast, a study using a homologous subtype C protein immunization reported induction of higher anti-Env antibody titers with aluminum-hydroxide (Ahydrogel) relative to Addavax, an MF59 analog, in rabbits(48).Collectively, these data indicate the importance of detailed studies to understand the context in which T_h1 responses are superior to mixed T_h1+2 responses and how viral versus DNA vectors and subunit proteins influence this paradigm.

Our findings raise the question of the mechanisms underlying the $D_{IP\text{-}10}Pro_{ALFQ}$ vaccine-mediated enhancement in T_{fh} responses. A few possibilities can be explored; IP-10 increases dendritic cell-T cell interactions, which could have favored T_{fh} differentiation(49). IP-10 also increases IL-6 production in B cells which is known to support T_{fh} differentiation and enhance plasma cell survival (50). This together with the potent immune stimulatory potential of MPLA+QS-21 boost may have synergized to enhance T_{fh} responses numerically and favored T_h1 differentiation program within T_{fh} cells (51). Indeed, GC T_{fh} cells induced following viral infections, where T_h1 inflammatory responses predominate, express Bcl-6, Tbx21, IFNG, and IL-21 consistent with the induction of T_h1-type T_{fh} cells (52). Transcriptomic analysis of T_{fh} cells following the 1st protein boost in the $D_{IP\text{-}10}$ P_{ALFQ} vaccine regimen show coordinate expression of T_h1 regulated genes as evidenced by enrichment of pathways related to IFNG signaling. It should be noted however that transcriptional analysis was only performed on 3 animals within the $D_{IP\text{-}10}$ P_{ALFQ} group with the highest magnitude antibody responses and

517 therefore may yield false positive targets and furthermore not be representative of the GC T_{fh} signature elicited
518 by the D_{IP-10} P_{ALFQ} vaccine regimen. Nonetheless, the higher relative expression of the T_h1 chemokine receptor
519 CXCR3 in GC T_{fh} cells and GC B cells, and CXCR3 ligands in sera lend support to the gene expression data.
520 Together, our transcriptomic and phenotypic data on T_{fh} cells indicate a role for adjuvant induced quantitative
521 (increased T_{fh} numbers) and qualitative (increased proportion of T_h1 T_{fh} cells) effects on antibody magnitude.
522 Mechanistic studies are needed to discern the respective contribution of increased T_{fh} numbers versus T_h1
523 skewing of T_{fh} cells on antibody responses as both these characteristics are inextricably linked in the current
524 study. Additionally, because our vaccine regimen differed by two components; IP-10 in the prime and ALFQ
525 during the boost further studies are needed to determine the specific role of the IP-10 prime versus ALFQ
526 boost in driving CD4 T_{fh} and antibody responses. This will enable us to address whether the T_h1 boost
527 synergized with the T_h1 prime to enhance antibody titers and functionality, or if a T_h1 prime/ T_h1 boost alone
528 would be sufficient to elicit the observed anti-Env antibody profiles.
529
530 While the D_{IP-10} P_{ALFQ} vaccine regimen increased magnitude of anti-Env IgG titers in the vaginal mucosa, which
531 correlated with decreased acquisition in each of the vaccine groups, our study was not powered to assess
532 protection from acquisition across the vaccine regimens. Furthermore, the lack of an unvaccinated control
533 group precludes determination of vaccine efficacy and is a major caveat to the interpretation of acquisition
534 outcomes. Therefore, more extensive larger scale studies are needed to assess whether the D_{IP-10} P_{ALFQ}
535 vaccine regimen induced protective antibodies with the capacity to mediate effective neutralization or antibody
536 effector functions at the vaginal mucosa. Notably, in contrast to a previous study showing increased risk of
537 intra-rectal acquisition with MF59 relative to an alum-adjuvanted protein immunization(46), the D_{IP-10} P_{ALFQ}
538 vaccine regimen did not increase the risk of vaginal acquisition in the present study. While these studies differ
539 in route of mucosal transmission, the difference in outcomes may also be attributed to timing of exposure
540 following final immunization i.e., 4 weeks in the previous study versus 20 weeks in the current study. It is
541 possible that the presence of higher frequency of CD4 T cell effectors at the rectal mucosa 4 weeks following
542 immunization increased acquisition risk, which could have contributed the observed differences in outcomes.
543 Indeed, higher frequencies of CCR5+ CD4 T cells in rectal mucosa were observed in vaccinated monkeys
544 experiencing breakthrough infections relative to those remaining uninfected following a low-dose intrarectal

545 challenge (53). Therefore, whether increased immunogenicity detracts from protection is an important safety
546 consideration in the use of T_h1 adjuvants and other highly immunogenic vaccine platforms(46). This is
547 particularly important as the HIV co-receptor CCR5 is primarily expressed on T_h1 cells (12). Nevertheless,
548 because T_h1 cells also produce CCR5 ligands, it is important to determine frequency of T_h17 cells at the
549 mucosal portals following immunization as T_h17 cells are preferential targets of infection within the vaginal
550 mucosa(54). Another consideration is that the studies were performed on females and did not encompass the
551 possible variability in vaccine response between sexes. Therefore, going forward, it is critical to determine and
552 confirm if a T_h1 vaccine regimen will also enhance antibody responses in males.
553
554 In addition to adjuvant-dependent modulation of T_{fh} responses, our IgG subclass results also support the
555 conclusion that the D_{IP-10} P_{ALFQ} and DP_{ALFA} vaccine regimens induced qualitatively different GC responses. This
556 is also the first study to show that adjuvants can dramatically impact the IgG antibody subclass profile in
557 rhesus macaques. We made the striking observation that while both vaccine regimens induced IgG1 antibodies
558 to gp120, the DP_{ALFA} regimen generated much greater IgG4 responses. The T_h2-promoting aluminum adjuvant
559 is most likely responsible for the increased IgG4 in DP_{ALFA} animals because both vaccine groups received ALF
560 liposomes. Rhesus IgG4 antibodies can mediate phagocytosis, but overall they appear to have poor effector
561 functions (55, 56) and the most functional IgG subclass in macaques has been reported to be IgG1 (56).
562 Humans immunized with an alum-formulated HIV-1 gp120 protein have been found to develop IgG1 and IgG4
563 but not IgG2 and IgG3 antibodies(57). However, important functional differences in IgG subclass antibodies
564 and FcγR biology between non-human primates and humans (58, 59), and the fact that rhesus IgG subclasses
565 are numbered by serum abundance not function preclude direct comparisons between species. Another
566 consideration is that differing antigen affinities between IgG subclasses to HIV-1 gp140 could confound
567 quantitation raising the possibility that subclass differences may be driven by differential affinities/epitope
568 specificities rather than differential magnitudes. Therefore, more conclusive studies are needed to evaluate
569 these possibilities.
570
571 Another notable observation was the induction, in D_{IP-10} P_{ALFQ} vaccinated animals, of a robust anti-Env vaginal
572 IgA response with an accompanying decline in serum IgA antibodies after the 2nd protein immunization. This

incongruity between vaginal and serum IgA responses was also observed in the DP_{ALFA} vaccine group, suggesting that ALF liposomes may have generated IgA plasmablasts that homed to the reproductive tract, or possibly T_h17-like T_{fh} cells which promote IgA responses in mucosal LNs (60) (61). The T_h1-biased ALF and ALFQ adjuvants have been reported to generate T_h17 responses in mice, with ALFQ being more effective and additionally generating IgA antibodies(62). Future studies of T_{fh} cell subsets and IgA plasma cells in mucosal LNs will be required to determine if our T_h1 vaccine regimen may have promoted IgA responses in the female reproductive tract, and in the rectum to a lesser extent, by generating T_h17 cells.

In summary, our findings demonstrate that T_h1-DNA prime substantially increases the frequency of Env-specific T_{fh} cells and that T_h1-Env protein boosting results in greater production of anti-Env IgG1 antibodies with enhanced magnitude, breadth, avidity, and function. How this regimen can be further optimized to significantly enhance and induce robust tier 2 neutralizing antibodies is an important question that warrants further study.

MATERIALS AND METHODS

Rhesus Macaques Twenty adult female colony-bred rhesus macaques (*Macaca mulatta*) were housed at the California National Primate Research Center and maintained in accordance with American Association for Accreditation of Laboratory Animal Care guidelines. All studies were approved by the University of California Davis Institutional Animal Care and Use Committee (IACUC). At study initiation, animals were 3.5 - 4.5 years of age with a median weight of 5.3 kg, were SIV- STLV- SRV-, had no history of dietary or pharmacological manipulation, and had intact ovaries.

Immunizations and challenge. DNA immunizations were administered via intradermal injection with electroporation utilizing the ICHOR TriGrid Array (Ichor Medical Systems) at weeks 0, 8, and 16. For each DNA immunization, two groups of 10 animals received 4 mg of the pGA2/JS2 plasmid DNA vector(63) encoding either SHIV C.1086 T/F Env + interferon-induced protein (IP)-10 (Group 1) or SHIV C.1086 T/F Env alone (Group 2). Details of the SHIV DNA construct have been described(64). At weeks 30 and 44, Group 1 animals received boosts with 100 μg C.ZA 1197MB gp140 protein (Immune Technology) adjuvanted with 100 μg MPLA +50 μg QS-21 (ALFQ) and Group 2 animals received 100 μg C.ZA 1197MB gp140 adjuvanted with 100 μg MPLA + 600 μg Aluminum (ALFA). The protein formulation (100 μg protein in 500μl formulation) was delivered in a 250 μl volume with 50 μg protein subcutaneously in each thigh during each of the two protein boosts. All animals were challenged at week 20 following the final protein immunization with 1:4 dilution of SHIV.C.CH505 (stock at 189 ng/ml) obtained from George Shaw and Nancy Miller. The virus was diluted 1:4 in RPMI to obtain a challenge volume of 1 ml. Animals were positioned in prone position and 1 ml syringe without needle was used to inoculate virus. Animals were challenged weekly, with 8 repeat doses or until virus was detected in plasma.

Adjuvants. Dimyristoyl phosphatidylcholine (DMPC) and dimyristoyl phosphatidylglycerol (DMPG) saturated phospholipids, cholesterol (Chol), and synthetic monophosphoryl lipid A (MPLA, 3D-PHAD) (Avanti Polar Lipids). DMPC and Chol were dissolved in chloroform, and DMPG and MPLA were dissolved in chloroform:methanol (9:1). Alhydrogel®, aluminum hydroxide (AH) in a gel suspension was purchased from Brenntag. The QS-21 saponin was purchased from Desert King International and was dissolved in Sorensen PBS, pH 5.6.

Army liposome formulations (ALF) containing DMPC, DMPG, Chol, and MPLA were prepared by the lipid deposition method. For vaccine preparations adjuvanted with ALFA, dissolved lipids were mixed in a molar ratio of 9:1:7.5:0.36 (DMPC:DMPG:Chol:MPLA) and dried by rotary evaporation followed by overnight desiccation. Liposomes were formed by molecular biology grade water (Quality Biological), microfluidized, and sterile filtered, followed by lyophilization. 100 μg of gp140 protein was adsorbed to 600 μg of Alhydrogel in PBS, pH 7.4, and incubated on a tilted roller at room temperature (RT) for 1 h prior to adding to lyophilized ALF. For vaccine preparations adjuvanted with ALFQ (ALF containing QS-21), lipids were mixed in a molar ratio of 9:1:12.2:0.36 (DMPC:DMPG:Chol:MPLA), dried, rehydrated by adding Sorensen PBS, pH 6.2, followed by microfluidization and filtration. gp140 was mixed with ALFQ in a 1:1 volume ratio. Each vaccine dose in 500 μl volume contained 100 μg MPLA (and 100 μg protein) and either 600 μg aluminum or 50 μg QS-21.

Specimen collection and processing. Lymph node (LN) biopsies were obtained 2 weeks following each of the protein boosts and were manually processed by disassociation through 100 μM cell strainers and washing in complete media, as described previously (12). Two weeks after the 3rd DNA immunization, fine needle aspirates of LN were obtained using a 22 gauge needle, as previously described (65). PBMCs were isolated from whole blood collected in CPT vacutainer tubes by density gradient centrifugation as previously described (12). For serum, coagulated blood was centrifuged at 800 g for 10 min to pellet clotted cells, followed by extraction of fluid and storage at -80°C. Rectal and vaginal secretions were collected using premoistened Weck-Cel sponges and eluted as described (66).

Serum IgG ELISA. Serum IgG titers against HIV-1 C.1086 Env gp140 and Gag (SIVmac 239) were determined by ELISA. In brief, 96-well microtiter plates with high binding capacity (Thermo Fisher) were coated

overnight at 4°C with 1 μg/mL C.1086 Env gp140C from the NIH AIDS Reagent Program (ARP) or with SIV239 Gag (Immune Tech) diluted in 0.1 M carbonate-bicarbonate buffer, pH 9.2. Plates were washed with PBS containing 0.1% Tween-20 (PBST) and blocked with 5% w/v nonfat dry milk in PBS for 2 h at RT followed by four washes with PBST. Standard (PG9 monoclonal antibody from the ARP) and serum samples were run at 3 dilutions/sample (1:50-1:450) in sample dilution buffer and incubated at RT for 2 h on a microplate shaker. After washing, the plate was incubated for 1 h with 1:10,000 HRP conjugated goat anti-monkey IgG (Nordic MUbio). The plates were washed and then developed with TMB substrate (Thermo Fisher) and the reaction was quenched with 2 N H_2SO_4 (Sigma). Absorbance was recorded at 450 nm with a reference filter at 570 nm using a Spectramax 5 plate reader (Molecular Devices). Baseline sera from each animal served as negative control and OD values 2-fold above baseline were considered positive and extrapolated to determine anti-Env antibody concentrations.

Sodium thiocyanate avidity assay. C.1086 Env gp140C-specific IgG antibody avidity was determined using a chaotropic displacement ELISA with NaSCN. Serum samples were incubated in duplicate at 6000 pg per well for 2 h at RT. The plate was washed five times. For the dissociation step, one well of each sample was manually treated with 100 μL of 2 M NaSCN (Sigma-Aldrich) to dissociate antigen-antibody complexes and a second well of the same sample was treated with PBS as a control. The plate was incubated for 15 min at RT, followed by washing three times. The plate was then developed as described above for the C.1086 gp140C ELISA. For each sample, antibody avidity was reported as an avidity index value (a percentage), which was calculated as the ratio of absorbance in the well treated with NaSCN to that in the well treated with PBS.

Biacore binding and avidity analysis. Binding and avidity determination were conducted using Surface Plasmon Resonance (SPR) Biacore 4000 system. The immobilizations were performed in 10 mM HEPES and 150 mM NaCl pH 7.4 using a standard amine coupling kit, as previously described (23, 67). The CM5-S series chip surface was activated with a 1:1 mixture of 0.4 M 1-ethyl-3-(3-dimethylaminopropyl) carbodimide hydrochloride (EDC) and 0.1 M N-hydroxysuccinimide (NHS) for 600 s (GE Healthcare). For the cyclic biotinylated V2 C.1086 peptide, 1 μM Streptavidin (Life Technologies) in 10 mM sodium acetate pH 4.5 (5,800 - 7,400 RU) was coupled for 720 s. The immobilized surface was then deactivated with 1.0 M ethanolamine-

Journal of Virology

HCl pH 8.5 for 600 s. Spot 3 in each flow cell was left unmodified to serve as a reference. Following surface deactivation, 0.06 - 1.5 µM cyclic biotinylated V2 C.1086 peptide was captured, resulting in two range of densities; high density (1,900 – 2,300 RU) and low/medium density (340 – 580 RU). For C.1086 gp140C, 0.56 – 15 µg/mL protein was immobilized directly on the sensor CM5 chip, resulting in four ranges of densities; very high density (9.800 – 10,100 RU); high density (3,400 – 4,100 RU); medium density (960 – 1,700 RU) and low density (240 - 670 RU). Following surface preparation, heat inactivated serum samples were diluted 1:50 in the running buffer (10 mM Hepes, 300 mM NaCl and 0.005% Tween 20, pH 7.4). The diluted samples were injected onto the V2 peptide or gp140 protein surface for 320 s followed by 1,800 s dissociation period. The bound surface was then enhanced with a 240 s injection of 30 µg/mL secondary antibody goat anti-monkey IgG. To regenerate the bound surface, 175 mM HCl was injected for 70 s. For each serum sample or controls, 4 - 8 replicates were collected at a rate of 10 Hz, with an analysis temperature of 25°C. All sample injections were conducted at a flow rate of 10 µL/min. Data analysis was performed using Biacore 4000 Evaluation Software 4.1 with double subtractions for unmodified surface and buffer for blank. The fitting was conducted using the dissociation mode integrated with the Evaluation software 4.1.

Binding Antibody Multiplex Assay (BAMA) and sodium citrate avidity assay. HIV-specific serum IgG BAMA was performed as previously described (68) with a panel of Env and V1V2 antigens: C.1086 gp140, CH505 TF gp140, Con S (group M consensus) gp140, and Con C (clade C consensus) gp140, gp70-V1V2 Clade B/Case A2 scaffolded protein. Samples were titrated in 5-fold serial dilutions starting at 1:80 and binding magnitude is reported as AUC. Positivity criteria (determined at dilution 1:80) was as follows: (1) MFI >100; (2) MFI > Ag-specific cutoff (95th percentile of all baseline binding per antigen); (3) MFI 3-fold > than that of the matched baseline before and after blank/MuLV subtraction. All BAMA and avidity assays were performed in a blinded fashion using magnetic beads. For avidity assays, samples were tested with and without sodium citrate (0.1 M, pH 3.0) at 2 dilutions for each antigen based on BAMA titration for maximum coverage of samples in the linear range of the assay. The dilutions were 1:80 and 1:400 for gp70-V1V2, 1:400 for C.1086 V1V2, 1:2000 for CH505TF gp140, 1:2000 for ConC gp140, and 1:10000 for C.1086 gp140 and ConS gp140. Antibody avidity is reported as avidity index, which was calculated as 100 x (MFI in the citrate-treated well/MFI in the untreated well). Avidity index is reported for sample-antigen combinations that were (1) identified as

704 positive responders in the IgG BAMA assay and (2) had an MFI within the linear range for the untreated
705 sample.
706
707 **Neutralization.** Neutralization assays were performed as previously described(69) using TZM-bl cells. We
708 measured neutralization activity against the tier 1 clade C pseudovirus MW965.26 using MLV-pseudotyped
709 virus as an indicator of non-HIV-specific activity in the assay. Neutralization titers were measured at week 2
710 and week 8 post 2nd protein boost and were considered to be positive for neutralizing antibody activity based
711 on the criterion of signal $\geq$3x detected against the MLV negative control virus. The majority of positive titers
712 detected were against the tier 1 virus MW965.26 with occasional very weak neutralization titers against the tier
713 2 C.1086_B2
714 and SHIV CH505.375H viruses.
715
716 **Antibody-dependent cellular cytotoxicity.** The rhesus CD16^{+} human KHYG-1 NK cell line (effector cells)
717 and CEM.NKR-CCR5-sLTR-Luc (target cells) were provided by Dr. David Evans (Univ of Wisconsin) and were
718 maintained in R10 culture medium consisting of RPMI 1640 supplemented with 10% fetal bovine serum, 25
719 mM HEPES, 2 mM L-glutamine, and 0.1 mg/ml Primocin (70, 71). The R10 for CD16^{+} KHYG-1 cells was
720 additionally supplemented with cyclosporine (CsA) and interleukin-2 (IL-2) at a concentration of 1 µg/ml and 5
721 U/mL, respectively.
722

723 Luciferase-based ADCC assays were carried out as previously described with some modifications (70). Two
724 million CEM.NKR-CCR5-sLTR-Luc target cells were spinoculated with SHIV.C.CH505.375H.dCT (38 ng p27)
725 for 2 h at 2,600 rpm at 30°C in the presence of 10 µg/mL polybrene. Subsequently, the target cell/virus mixture
726 was incubated overnight at 37°C in 5% CO_2. The next day, virus was removed and cells were incubated for
727 another 72 h prior to the ADCC assay. For the ADCC assay, serum: effector cells: target cells were plated in a
728 1:1:1 volumetric ratio. Serum was heat inactivated and diluted (1:50 dilution in R10 containing 10 U IL-2 per
729 mL, with no CsA), mixed with PBS-washed, infected target cells (1 x 10^4 cells per well), and effector cells (5 x
730 10^4 cells per well). Serum and cells were incubated overnight at 37°C in 5% CO_2. Plates were then centrifuged
731 at 1,800 rpm for 5 min at room temperature and 100 uL of the supernatant was removed. The cell pellets were
732 resuspended and mixed with 50 µl of the luciferase substrate reagent BriteLite Plus (Perkin Elmer). Relative
733 light units (RLUs) were recorded in black 96-well plates according to the manufacturer's instructions using a
734 Synergy 2 microplate luminometer (BioTek). Percent ADCC activity of each tested serum sample (week 2 and
735 week 8 post 2nd protein) was measured as the reduction in RLUs compared to the animal's week 0 pre-immune
736 serum (100% RLU). All samples were tested in triplicate and experiments were performed twice.
737
738 **Antibody Dependent Phagocytosis.** Serum antibodies were tested for ability to enhance phagocytosis of
739 gp120 expressing beads by THP-1 cells using methods similar to those previously described(69). Briefly, 5 µL
740 of 1 µm avidin-coated Fluorospheres (Invitrogen) were labeled with 2 µg biotinylated anti-His tag antibody
741 (Pierce), then 3.5 µg His-tagged Clade C gp120 Du151 protein (Immune Technologies) per plate. The gp120
742 beads and triplicate 5-fold dilutions of heat-inactivated serum in a 50 µL volume were then pre-incubated at
743 37˚C in V-bottom plates. After 1 h, 2 x 10^4 THP-1 cells in 50 µL were added to each well. After 5 h at 37˚C in
744 5% CO_2, the cells were washed in Ca^{+2} and Mg^{+2} -free DPBS and resuspended in 180 µL of warm 0.12%
745 Trypsin/EDTA. After 5 min at 37˚C, the trypsin was removed and the cells were resuspended in 1%
746 paraformaldehyde. Fluorescence was evaluated using a FACS Canto (BD Biosciences) and Flow-jo software.
747 Phagocytosis was measured by multiplying the percent fluorescent cells by their median fluorescence intensity.
748 The phagocytic score was then calculated by dividing phagocytosis of test samples by the average
749 phagocytosis measured with preimmune serum.
750

751 **IgG subclass antibodies**. Ten rows of a 96-well Immulon 4 microtiter plate (VWR) were coated overnight at
752 4˚C with 50 ng per well of C.1086 gp120 Δ7 K160N protein (72) in PBS. The remaining 2 rows were coated
753 with duplicate 2-fold serial dilutions of rhesus IgG1, IgG2, IgG3 or IgG4 (Nonhuman Primate Reagent Program)
754 starting at 25 ng/mL in PBS to generate a standard curve. Plates were washed with PBS containing 0.05%
755 Tween 20 and blocked for 30 min at RT with reagent buffer (0.1% bovine serum albumin in wash buffer). Two-
756 or three-fold dilutions of serum in reagent buffer were then added to the wells coated with gp120. Reagent
757 buffer was added to wells coated with standard. Following overnight storage at 4˚C, the plate was washed and
758 reacted for 1 h at 37˚C with 1 µg/mL of the relevant monoclonal antibody from the Nonhuman Primate Reagent
759 Resource: anti-rhesus IgG1 (mouse IgG2a clone 3C10.3), anti-rhesus IgG2 (mouse IgG1 clone 3C10), anti-
760 rhesus IgG3 (mouse IgG1 clone 2G11) or anti-rhesus IgG4 (mouse IgG1 clone 7A8). These antibodies were
761 raised to react specifically with the respective rhesus IgG subclass and show negligible reactivity to other
762 subclasses and the specificity of 7A8 was further confirmed in our lab. The plate was then consecutively
763 washed and treated with 100ng/mL of biotinylated goat anti-mouse IgG1 or IgG2a for 1 h at 37˚C, neutralite-
764 avidin peroxidase for 30 min at RT, and TMB (all from SouthernBiotech). Absorbance was recorded at 370 nm.
765 SoftMax Pro software (Molecular Devices) was used to to construct a standard curve and determine
766 concentrations of antibody. Preimmune serum samples had < 10ng/mL of antibody in these assays.
767
768 **Mucosal antibodies and serum IgA.** BAMA with C.1086 gp140 K160N-labeled magnetic beads (MagPlex,
769 BioRad) was used as previously described (72) to measure concentrations of antigen-specific IgG in
770 secretions and IgA in both secretions and serum depleted of IgG. Briefly, beads reacted with dilutions of
771 standard (73) and specimens at 1100 rpm and 4˚C overnight were washed and developed with biotinylated
772 anti-monkey IgG or -monkey IgA (Rockland) followed by Phycoerythrin-labeled Neutralite avidin
773 (SouthernBiotech). Construction of standard curves and interpolation of antibody concentrations was done
774 using Bioplex Manager software after measurement of fluorescence in a Bioplex 200 (BioRad). Concentrations
775 of gp120-specific IgG or IgA in secretions were divided by the total IgG or IgA measured in the sample by
776 ELISA (74) to obtain the specific activity (ng IgG or IgA antibody per µg total IgG or IgA).
777

Activation induced Marker (AIM) assay. Cells were stimulated with overlapping peptide pools of HIV consensus C and HIV-1 C.1086 Env gp140C protein; and SIV239 Gag in AIM media as previously described (30). All antigens were used at a final concentration of 2 μg/mL in a stimulation cocktail made with using 0.2 μg of CD28 and 0.2 μg CD49d costimulatory antibodies per test. Unstimulated controls were treated with volume-controlled DMSO (Sigma-Aldrich). Tubes were incubated in 5% CO_2 at 37°C overnight. Following an 18 h stimulation, the cells were stained, fixed, and acquired the same day. Phenotype panel on LNs and PBMCs was performed using standard flow cytometry assays(12).

Serum cytokines. A Legendplex assay (Biolegend) was performed to evaluate cytokines in rhesus macaque sera. The assay was performed according to the manufacturer's protocol. Samples were acquired on a BD LSR Fortessa cell analyzer.

Flow cytometry and cell sorting. Cell staining and sorting was performed as previously described(12). Fluorescence was measured using a BD FACSymphony with FACS Diva version 8.0.1 software. Compensation, gating and analysis were performed using FlowJo (Versions 9 and 10). Cell sorting was performed using a BD FACSAria III. Reagents used for flow cytometry are listed in Table 1.

RNA Sequencing and Bioinformatics. RNA was extracted from sorted subsets and DNA-free RNA was quantified and assessed for quality prior to sequencing. RNA samples with visible peaks, 260/280 ratio between 1.8 to 2.1, and RNA integrity number of greater than 7 were sequenced using Batch-Tag-Seq Gene Expression Profiling on the Illumina HiSeq sequencer at the DNA Technologies & Expression Analysis Core Laboratory at the UC Davis Genome Center. Samples were barcoded and run in a single HiSeq lane. Quality of data were verified using the Illumina SAV viewer; this included verifying low error rates based on alignments of the standard Illumina PhiX spike, and removal of PCR duplicates after alignments. Adapter trimming, QC of sequencing data & demultiplexing was performed by the UC Davis Bioinformatics Core. After read filtering, reads were mapped to a reference genome using HISAT-aligner. On average 82.17% (~55-61% uniquely mapped) reads were mapped, and the uniformity of the mapping result for each sample indicated comparability between samples. Prior to differential gene expression analysis, genes with fewer than 40

806 counts per million reads were filtered, leaving 7,086 genes. Differential expression analyses were conducted
807 using the limma-voom Bioconductor pipeline (32).
808
809 **Statistical analysis.** Statistical analysis was performed using GraphPad Prism 7. Results between groups
810 were compared using the two-tailed nonparametric Mann-Whitney rank sum test. Within group comparisons,
811 such as antibody levels at different time points, were done using the two-tailed Wilcoxon matched-pairs signed
812 rank test. For correlation analysis, the two-tailed Spearman rank correlation test was used.
813

814 **Acknowledgements** The authors are grateful to the primate center staff Wilhelm Von Morgenland, Miles
815 Christensen, Irma Cazares-Shaw, Vanessa Bakula for immunizations and animal sampling. The authors
816 acknowledge the contribution of Abigail Spinner for assistance with sorting of LN CD4 subsets, Ryan Mathura,
817 and Tam Huynh for serum IgG BAMA and avidity index assays, and Robert L. Wilson with mucosal antibody
818 measurements. Rhesus subclass specific antibodies were provided by the Nonhuman Primate Reagent
819 Resource with support from grant U24 AI126683. RNA sequencing was performed at the DNA Technologies &
820 Expression Analysis Core Laboratory and differential gene analysis was performed by the Bioinformatics Core
821 at the UC Davis Genome Center Env and V1V2 scaffolded proteins used in BAMA were designed and
822 provided by the Protein Production Facility of Duke Human Vaccine Institute under the direction of Drs.
823 Peacock and Haynes, and Dr. Abe Pinter, respectively. We thank George Shaw and Nancy Miller for the
824 SHIV.C.CH505 virus.
825
826 This work was partially supported by a cooperative agreement (W81XWH-18-2-0040) between the Henry M.
827 Jackson Foundation for the Advancement of Military Medicine, Inc., and the U.S. Department of Defense
828 (DoD). Material has been reviewed by the Walter Reed Army Institute of Research. There is no objection to its
829 presentation and/or publication. The opinions or assertions contained herein are the private views of the
830 author, and are not to be construed as official, or as reflecting true views of the Department of the Army or the
831 Department of Defense.
832
833 RRA and SSI have a patent pending for the DNAIP10 construct.

834

835 **FIGURE LEGENDS**

836 **Figure 1**. **Immunization schedule for subtype C HIV-1 Envelope DNA prime and protein boost vaccine**
837 **regimen**. (**A**) Flow cytometric plots illustrate expression of HIV Env, SIV Gag, and IP-10 by 293T cells
838 transfected with DNA and DNA_{IP-10} plasmids. Grey overlay shows expression in non-transfected cells. (**B**)
839 Surface expression of HIV Env based on detection with a panel of monoclonal antibodies as indicated. (**C**) IP-
840 10 concentrations in supernatants of transfected 293T cells show accumulation of IP-10 following transfection
841 with DNA_{IP-10}. (**D**) Immunization schedule. Two groups of 10 rhesus macaques each were immunized three
842 times with DNA followed by two immunizations with protein. DNA was delivered intradermally and three
843 seconds later electrical pulses were delivered around the injection site using the ICHOR TriGrid Array. Group 1
844 animals (n=10) received DNA plasmid expressing IP-10 and an ALFQ-adjuvanted C.ZA gp140 boost (D_{IP-}
845 $_{10}Pro_{ALFQ}$). Group 2 (n=10) animals were immunized with DNA and boosted with ALFA-adjuvanted C.ZA gp140
846 protein (DP_{ALFA}). (**E**) Induction of IP-10, I-TAC, IL-6, and RANTES in serum after the 1st protein immunization
847 in both vaccine regimens. Significance was tested by Mann-Whitney; * $p<0.05$, ** $p \leq 0.01$, *** $p \leq 0.001$.

848

849 **Figure 2. $D_{IP-10}Protein_{ALFQ}$ vaccine induces robust anti-Env serum IgG antibody titers with cross-clade**
850 **breadth. (A)** Kinetics of the C.1086 anti-gp140 IgG response measured by BAMA in serum at weeks 0, 2, and
851 8 following each protein boost. The right panel shows scatter plot values for each animal at weeks 0, 2, and 8
852 post 2nd protein boost. **(B)** Kinetics of the C.1086 gp140-specific anti-Env IgG response measured by ELISA
853 after the 2nd protein boost. The right panel shows titers for each individual animal. BAMA assay was used to
854 measure responses against **(C)** CH505 gp140, **(D)** Con C gp140 **(E)** Con S gp140 and **(F)** gp70-V1V2 Case
855 A2. (**G**) Fold change in antibody titers at indicated time points after the 2nd protein boost relative to the 1st.
856 Animals receiving the DP_{ALFA} vaccine are represented by blue circles and animals receiving the $D_{IP-10}P_{ALFQ}$
857 vaccine by red circles. Kinetic data show geometric means. Vertical dotted lines show immunization time
858 points. In dot plots, geometric means are indicated as horizontal lines. Statistical significance across vaccine
859 regimens was tested using the Mann-Whitney U test; * $p \leq 0.05$, ** $p \leq 0.01$, *** $p \leq 0.001$, **** $p \leq 0.0001$.

860

Figure 3. D_{IP-10} $Protein_{ALFQ}$ vaccine elicits high avidity anti-Env antibody with ADCC and ADP activities. **(A)** Surface Plasmon Resonance (SPR) was used to determine the avidity index (AI) in serum at 2 weeks after the final DNA immunization and each protein boost using C.1086 gp140 protein immobilized onto sensor chips. Violin plots show median (bolded line) and interquartile range (dashed lines) in both vaccine groups with each sample run in quadruplicate. Lower values indicate higher avidity. **(B)** SPR-based AI values in the two vaccine regimens over time. **(C)** shows significantly higher IgG values in D_{IP-10} $P_{ALFQ.}$ at 2 weeks post 2nd protein boost (expressed as relative units, as measured by SPR) and higher avidity after normalizing avidity to gp140 IgG RU. Lower values indicate higher avidity. AI measured against C.1086 gp140 using (**D**) 2M sodium thiocyanate and (**E)** 0.1M sodium citrate at week 8 after 2nd protein boost. AI against (**F**) Con C and (**G**) Con S gp140 measured using 0.1M sodium citrate at week 8 post 2nd protein boost. (**H**) Serum neutralizing antibodies were assessed against tier 1A (MW965.26) pseudovirus and the 50% infective dose (ID50) was determined. (**I**) ADCC activity against SHIV CH505 infected target cells; data are represented with week 0 serum ADCC values normalized at 0% (dashed grey line) (**J**) ADP using Clade C Du151 gp120-coated beads was measured using sera from week 8 post 2nd protein boost at serum dilutions ranging from 1:100 to 1:2500. (**K**) Individual ADP scores at the 1:500 serum dilution. (**L**) C.1086 gp120-specific IgG subclass analysis was performed by ELISA using serum collected 8 weeks after the 2nd protein boost. (**M**) IgG1/IgG4 ratio across vaccine groups at week 8 post 2nd protein boost. Statistical significance across vaccine regimens was examined using the Mann-Whitney U test and within group differences over time were tested using Wilcoxon matched-pairs signed rank test; *$p \leq 0.05$, **$p \leq 0.01$, *** $p \leq 0.001$, **** $p \leq 0.0001$.

Figure 4. DNA_{IP-10} $Protein_{ALFQ}$ vaccine elicits robust anti-Env antibody in vaginal and rectal mucosal secretions. Concentrations of anti-C.1086 gp140 IgG and IgA in secretions were measured by BAMA and adjusted in accordance with the total IgG and IgA, respectively, to obtain the specific activity. (**A, B**) Development of gp140-specific IgG and (**C,D**) IgA in vaginal and rectal secretions. (**E**) Kinetics of the C.1086 gp140-specific IgA response in serum. Horizontal dashed lines represent the cut-off for significance. Kinetic data show geometric means. Vertical dotted lines show immunization time points. In dot plots, data post 2nd protein are shown and geometric means are indicated as horizontal lines. (**F**) Kaplan-Meier plot showing acquisition rates following eight repeat intra-vaginal challenges with SHIV.C.CH505. (**G**) vaginal anti-gp140

IgG concentrations at week 16 post 2nd protein boost correlated with delay in acquisition in infected animals in both vaccine regimens (D_{IP-10} P_{ALFQ} vaccine regimen, n = 7; DP_{ALFA} vaccine regimen, n = 10). Statistical significance was tested using unpaired, two-tailed Mann-Whitney U test; *$p \leq 0.05$, **$p \leq 0.01$, *** $p \leq 0.001$, **** $p \leq 0.0001$, and correlations with a Spearman rank correlation

Figure 5. D_{IP-10} $Protein_{ALFQ}$ vaccine induces Env-specific T cells and T_{fh} cells in blood. (A) Gating strategy to identify $CXCR5^+$ $OX40^+$ $CD25^+$ Env-specific T_{fh} cells within PBMC after stimulation with both whole C.1086 gp140 protein and pooled overlapping peptides representing Con C gp140. Flow plot illustrating responses following stimulation with Env or volume-controlled DMSO (NS). **(B)** Frequency of Env-specific CD4 T cells at week 1 post 1st protein boost.

Figure 6. D_{IP-10} $Protein_{ALFQ}$ vaccine induces GC T_{fh} cells with distinctive T_h1 signatures. (A) Gating strategy to identify GC T_{fh} cells and GC B cells in LN at 2 weeks post 1st protein boost. Histograms show higher relative expression of Bcl-6 and ICOS in GC T_{fh} cells (red) compared to naive CD4 T cells (grey). Expression in GC B cells is shown in purple. **(B)** Total IgG was measured in *ex vivo* co-culture experiments with sorted GC T_{fh} cells and autologous LN B cells to demonstrate B helper capacity of the T_{fh} cells. (**C)** Frequencies of GC T_{fh} cells in LN at specified time points, symbols indicate significant differences from baseline for protein 1 and day 0 for protein 2. (**D**) Dot plot illustrating higher frequencies of GC B cells in the T_h1 vaccine group, and correlations between frequencies of GC T_{fh} cells and GC B cells or Env-specific Tfh cells in in LN. Frequencies of Env-specific CD4 T cells in LN (D, figure on right) correlate with GC T_{fh} cells. **(E)** Histogram illustrating relative CXCR3 expression in GC T_{fh} cells (red) and GC B cells (purple). The dot plot shows significantly higher CXCR3 expression on GC T_{fh} cells in the T_h1 vaccine group. Serum antibody titers at week 18 after the 2nd protein boost correlate with frequency of GC T_{fh} cells and proportion of CXCR3-expressing GC T_{fh} cells at 2 weeks after the 1st protein boost. **(F)** The dot plot shows significantly higher CXCR3 expression on GC B cells from animals in the T_h1 vaccine group. Flow plot illustrates higher expression of CXCR3 on T-bet+ memory B cells. (**G)** Log fold change values of key T_{fh} and T_h1 genes in T_{fh} and memory T_{fh} cells in lymph node of T_h1 vaccinated animals (p adj <0.05). (**H)** Heatmap shows expression of genes differentially expressed in T_{fh} cells relative to naive across four sorted CD4 subsets. Blue and red colors represent relative high and low log2

917 gene expression values, respectively. For construction of heat maps log 2 gene expression (counts per million
918 or CPM) for the most differentially expressed genes in T_{fh} versus naive comparison, selected by threshold of p-
919 adjusted value <= 0.05. Statistical significance was tested using unpaired, two-tailed Mann-Whitney U test.
920 Spearman coefficient of correlation values were computed to determine associations; * $p<0.05$, **** $p \leq 0.0001$.
921

922 **Figure 7. DNA_{IP-10} immunization induces systemic expansion of pro-inflammatory monocytes and**
923 **enhances GC T_{fh} responses. (A)** Gating strategy to identify activated $CXCR5^+$ CD4 T cells in blood on day 0
924 and day 14 following the 3rd DNA immunization, and transient accumulation of $ICOS^+$ $PD\text{-}1^+$ $CXCR5^+$ cells in
925 blood of all animals (n=20) when expressed as relative frequencies (left) or absolute counts (right). **(B)** Kinetics
926 of the SIV239 anti-Gag IgG response and **(C)** C.1086 gp140-specific anti-Env IgG response measured by
927 ELISA after DNA immunization at indicated time points. Significance indicated for all time points relative to
928 baseline titers. **(D)** shows Gag-specific CD4 T cell responses measured at week 1 post DNA3 using AIM and
929 ICS (IFNG+TNFA+)-based assays. **(E)** Gating strategy to identify inflammatory $CD14^+CD16^+$ monocytes in
930 blood. (**F**) Appearance of $CD14^+CD16^+$ monocytes following the 3rd DNA immunization. **(G** Comparison of pro-
931 inflammatory monocytes in blood of DNA and DNA-IP-10 primed animals. **(H)** Frequencies of GC T_{fh} cells in
932 fine needle aspirates of draining LNs from DNA and DNA-IP-10 primed animals on day 14 after the 3rd DNA
933 immunization. **(I)** Spearman rank correlation between frequencies of pro-inflammatory monocytes in blood on
934 day 3 and C.1086C gp140 IgG antibodies in serum on week 8 following the 2nd protein boost**.** Between group
935 differences were assessed using the Mann-Whitney U test. * $p< 0.05$, ***, $p \leq 0.001$, **** $p \leq 0.0001$.
936
937
938
939
940
941
942
943
944
945
946
947
948
949
950
951
952

REFERENCES

1. **Breitfeld D, Ohl L, Kremmer E, Ellwart J, Sallusto F, Lipp M, Forster R.** 2000. Follicular B helper T cells express CXC chemokine receptor 5, localize to B cell follicles, and support immunoglobulin production. J Exp Med **192:**1545-1552.
2. **MacLennan IC.** 1994. Germinal centers. Annu Rev Immunol **12:**117-139.
3. **Crotty S.** 2019. T Follicular Helper Cell Biology: A Decade of Discovery and Diseases. Immunity **50:**1132-1148.
4. **Aljurayyan A, Puksuriwong S, Ahmed M, Sharma R, Krishnan M, Sood S, Davies K, Rajashekar D, Leong S, McNamara PS, Gordon S, Zhang Q.** 2018. Activation and Induction of Antigen-Specific T Follicular Helper Cells Play a Critical Role in Live-Attenuated Influenza Vaccine-Induced Human Mucosal Anti-influenza Antibody Response. J Virol **92**.
5. **De Boer RJ, Perelson AS.** 2017. How Germinal Centers Evolve Broadly Neutralizing Antibodies: the Breadth of the Follicular Helper T Cell Response. J Virol **91**.
6. **Bannard O, Cyster JG.** 2017. Germinal centers: programmed for affinity maturation and antibody diversification. Curr Opin Immunol **45:**21-30.
7. **Song W, Craft J.** 2019. T follicular helper cell heterogeneity: Time, space, and function. Immunol Rev **288:**85-96.
8. **Schmitt N, Ueno H.** 2013. Blood Tfh cells come with colors. Immunity **39:**629-630.
9. **Schmitt N, Ueno H.** 2015. Regulation of human helper T cell subset differentiation by cytokines. Curr Opin Immunol **34:**130-136.
10. **Bentebibel SE, Khurana S, Schmitt N, Kurup P, Mueller C, Obermoser G, Palucka AK, Albrecht RA, Garcia-Sastre A, Golding H, Ueno H.** 2016. ICOS(+)PD-1(+)CXCR3(+) T follicular helper cells contribute to the generation of high-avidity antibodies following influenza vaccination. Sci Rep **6:**26494.
11. **Baiyegunhi O, Ndlovu B, Ogunshola F, Ismail N, Walker BD, Ndung'u T, Ndhlovu ZM.** 2018. Frequencies of Circulating Th1-Biased T Follicular Helper Cells in Acute HIV-1 Infection Correlate with the Development of HIV-Specific Antibody Responses and Lower Set Point Viral Load. J Virol **92**.
12. **Iyer SS, Gangadhara S, Victor B, Gomez R, Basu R, Hong JJ, Labranche C, Montefiori DC, Villinger F, Moss B, Amara RR.** 2015. Codelivery of Envelope Protein in Alum with MVA Vaccine Induces CXCR3-Biased CXCR5+ and CXCR5- CD4 T Cell Responses in Rhesus Macaques. J Immunol **195:**994-1005.
13. **Haynes BF, Gilbert PB, McElrath MJ, Zolla-Pazner S, Tomaras GD, Alam SM, Evans DT, Montefiori DC, Karnasuta C, Sutthent R, Liao HX, DeVico AL, Lewis GK, Williams C, Pinter A, Fong Y, Janes H, DeCamp A, Huang Y, Rao M, Billings E, Karasavvas N, Robb ML, Ngauy V, de Souza MS, Paris R, Ferrari G, Bailer RT, Soderberg KA, Andrews C, Berman PW, Frahm N, De Rosa SC, Alpert MD, Yates NL, Shen X, Koup RA, Pitisuttithum P, Kaewkungwal J, Nitayaphan S, Rerks-Ngarm S, Michael NL, Kim JH.** 2012. Immune-correlates analysis of an HIV-1 vaccine efficacy trial. N Engl J Med **366:**1275-1286.
14. **Kim JH, Excler JL, Michael NL.** 2015. Lessons from the RV144 Thai phase III HIV-1 vaccine trial and the search for correlates of protection. Annu Rev Med **66:**423-437.
15. **Ding BB, Bi E, Chen H, Yu JJ, Ye BH.** 2013. IL-21 and CD40L synergistically promote plasma cell differentiation through upregulation of Blimp-1 in human B cells. J Immunol **190:**1827-1836.
16. **Yusuf I, Kageyama R, Monticelli L, Johnston RJ, Ditoro D, Hansen K, Barnett B, Crotty S.** 2010. Germinal center T follicular helper cell IL-4 production is dependent on signaling lymphocytic activation molecule receptor (CD150). J Immunol **185:**190-202.
17. **Lin L, Finak G, Ushey K, Seshadri C, Hawn TR, Frahm N, Scriba TJ, Mahomed H, Hanekom W, Bart PA, Pantaleo G, Tomaras GD, Rerks-Ngarm S, Kaewkungwal J, Nitayaphan S, Pitisuttithum P, Michael NL, Kim JH, Robb ML, O'Connell RJ, Karasavvas N, Gilbert P, S CDR, McElrath MJ, Gottardo R.** 2015. COMPASS identifies T-cell subsets correlated with clinical outcomes. Nat Biotechnol **33:**610-616.
18. **Pissani F, Schulte B, Eller MA, Schultz BT, Ratto-Kim S, Marovich M, Thongcharoen P, Sriplienchan S, Rerks-Ngarm S, Pitisuttithum P, Esser S, Alter G, Robb ML, Kim JH, Michael NL, Streeck H.** 2018. Modulation of Vaccine-Induced CD4 T Cell Functional Profiles by Changes in Components of HIV Vaccine Regimens in Humans. J Virol **92**.

19. **Schultz BT, Teigler JE, Pissani F, Oster AF, Kranias G, Alter G, Marovich M, Eller MA, Dittmer U, Robb ML, Kim JH, Michael NL, Bolton D, Streeck H.** 2016. Circulating HIV-Specific Interleukin-21(+)CD4(+) T Cells Represent Peripheral Tfh Cells with Antigen-Dependent Helper Functions. Immunity **44:**167-178.
20. **Matyas GR, Mayorov AV, Rice KC, Jacobson AE, Cheng K, Iyer MR, Li F, Beck Z, Janda KD, Alving CR.** 2013. Liposomes containing monophosphoryl lipid A: a potent adjuvant system for inducing antibodies to heroin hapten analogs. Vaccine **31:**2804-2810.
21. **Beck Z, Torres OB, Matyas GR, Lanar DE, Alving CR.** 2018. Immune response to antigen adsorbed to aluminum hydroxide particles: Effects of co-adsorption of ALF or ALFQ adjuvant to the aluminum-antigen complex. J Control Release **275:**12-19.
22. **Pollara J, Jones DI, Huffman T, Edwards RW, Dennis M, Li SH, Jha S, Goodman D, Kumar A, LaBranche CC, Montefiori DC, Fouda GG, Hope TJ, Tomaras GD, Staats HF, Ferrari G, Permar SR.** 2019. Bridging Vaccine-Induced HIV-1 Neutralizing and Effector Antibody Responses in Rabbit and Rhesus Macaque Animal Models. J Virol **93**.
23. **Wen Y, Trinh HV, Linton CE, Tani C, Norais N, Martinez-Guzman D, Ramesh P, Sun Y, Situ F, Karaca-Griffin S, Hamlin C, Onkar S, Tian S, Hilt S, Malyala P, Lodaya R, Li N, Otten G, Palladino G, Friedrich K, Aggarwal Y, LaBranche C, Duffy R, Shen X, Tomaras GD, Montefiori DC, Fulp W, Gottardo R, Burke B, Ulmer JB, Zolla-Pazner S, Liao HX, Haynes BF, Michael NL, Kim JH, Rao M, O'Connell RJ, Carfi A, Barnett SW.** 2018. Generation and characterization of a bivalent protein boost for future clinical trials: HIV-1 subtypes CR01_AE and B gp120 antigens with a potent adjuvant. PLoS One **13:**e0194266.
24. **Qualls ZM, Choudhary A, Honnen W, Prattipati R, Robinson JE, Pinter A.** 2018. Identification of Novel Structural Determinants in MW965 Env That Regulate the Neutralization Phenotype and Conformational Masking Potential of Primary HIV-1 Isolates. J Virol **92**.
25. **Asbach B, Kibler KV, Kostler J, Perdiguero B, Yates NL, Stanfield-Oakley S, Tomaras GD, Kao SF, Foulds KE, Roederer M, Seaman MS, Montefiori DC, Parks R, Ferrari G, Forthal DN, Phogat S, Tartaglia J, Barnett SW, Self SG, Gottardo R, Cristillo AD, Weiss DE, Galmin L, Ding S, Heeney JL, Esteban M, Jacobs BL, Pantaleo G, Wagner R.** 2019. Priming with a Potent HIV-1 DNA Vaccine Frames the Quality of Immune Responses prior to a Poxvirus and Protein Boost. J Virol **93**.
26. **Forthal DN, Finzi A.** 2018. Antibody-dependent cellular cytotoxicity in HIV infection. AIDS **32:**2439-2451.
27. **Worley MJ, Fei K, Lopez-Denman AJ, Kelleher AD, Kent SJ, Chung AW.** 2018. Neutrophils mediate HIV-specific antibody-dependent phagocytosis and ADCC. J Immunol Methods **457:**41-52.
28. **Huang Y, Ferrari G, Alter G, Forthal DN, Kappes JC, Lewis GK, Love JC, Borate B, Harris L, Greene K, Gao H, Phan TB, Landucci G, Goods BA, Dowell KG, Cheng HD, Bailey-Kellogg C, Montefiori DC, Ackerman ME.** 2016. Diversity of Antiviral IgG Effector Activities Observed in HIV-Infected and Vaccinated Subjects. J Immunol **197:**4603-4612.
29. **Crowley AR, Ackerman ME.** 2019. Mind the Gap: How Interspecies Variability in IgG and Its Receptors May Complicate Comparisons of Human and Non-human Primate Effector Function. Front Immunol **10:**697.
30. **Havenar-Daughton C, Reiss SM, Carnathan DG, Wu JE, Kendric K, Torrents de la Pena A, Kasturi SP, Dan JM, Bothwell M, Sanders RW, Pulendran B, Silvestri G, Crotty S.** 2016. Cytokine-Independent Detection of Antigen-Specific Germinal Center T Follicular Helper Cells in Immunized Nonhuman Primates Using a Live Cell Activation-Induced Marker Technique. J Immunol **197:**994-1002.
31. **Stone SL, Peel JN, Scharer CD, Risley CA, Chisolm DA, Schultz MD, Yu B, Ballesteros-Tato A, Wojciechowski W, Mousseau B, Misra RS, Hanidu A, Jiang H, Qi Z, Boss JM, Randall TD, Brodeur SR, Goldrath AW, Weinmann AS, Rosenberg AF, Lund FE.** 2019. T-bet Transcription Factor Promotes Antibody-Secreting Cell Differentiation by Limiting the Inflammatory Effects of IFN-gamma on B Cells. Immunity **50:**1172-1187 e1177.
32. **Ritchie ME, Phipson B, Wu D, Hu Y, Law CW, Shi W, Smyth GK.** 2015. limma powers differential expression analyses for RNA-sequencing and microarray studies. Nucleic Acids Res **43:**e47.
33. **Kumanogoh A, Shikina T, Suzuki K, Uematsu S, Yukawa K, Kashiwamura S, Tsutsui H, Yamamoto M, Takamatsu H, Ko-Mitamura EP, Takegahara N, Marukawa S, Ishida I, Morishita H, Prasad DV, Tamura M, Mizui M, Toyofuku T, Akira S, Takeda K, Okabe M, Kikutani H.** 2005.

Nonredundant roles of Sema4A in the immune system: defective T cell priming and Th1/Th2 regulation in Sema4A-deficient mice. Immunity **22:**305-316.

34. **Li G, Liang X, Lotze MT.** 2013. HMGB1: The Central Cytokine for All Lymphoid Cells. Front Immunol **4:**68.
35. **Dinarello CA.** 1999. IL-18: A TH1-inducing, proinflammatory cytokine and new member of the IL-1 family. J Allergy Clin Immunol **103:**11-24.
36. **Chin AI, Dempsey PW, Bruhn K, Miller JF, Xu Y, Cheng G.** 2002. Involvement of receptor-interacting protein 2 in innate and adaptive immune responses. Nature **416:**190-194.
37. **Kwissa M, Nakaya HI, Oluoch H, Pulendran B.** 2012. Distinct TLR adjuvants differentially stimulate systemic and local innate immune responses in nonhuman primates. Blood **119:**2044-2055.
38. **Barbet G, Sander LE, Geswell M, Leonardi I, Cerutti A, Iliev I, Blander JM.** 2018. Sensing Microbial Viability through Bacterial RNA Augments T Follicular Helper Cell and Antibody Responses. Immunity **48:**584-598 e585.
39. **Ben-Sasson SZ, Hu-Li J, Quiel J, Cauchetaux S, Ratner M, Shapira I, Dinarello CA, Paul WE.** 2009. IL-1 acts directly on CD4 T cells to enhance their antigen-driven expansion and differentiation. Proc Natl Acad Sci U S A **106:**7119-7124.
40. **Khoruts A, Osness RE, Jenkins MK.** 2004. IL-1 acts on antigen-presenting cells to enhance the in vivo proliferation of antigen-stimulated naive CD4 T cells via a CD28-dependent mechanism that does not involve increased expression of CD28 ligands. Eur J Immunol **34:**1085-1090.
41. **Bart PA, Huang Y, Karuna ST, Chappuis S, Gaillard J, Kochar N, Shen X, Allen MA, Ding S, Hural J, Liao HX, Haynes BF, Graham BS, Gilbert PB, McElrath MJ, Montefiori DC, Tomaras GD, Pantaleo G, Frahm N.** 2014. HIV-specific humoral responses benefit from stronger prime in phase Ib clinical trial. J Clin Invest **124:**4843-4856.
42. **Hu X, Valentin A, Dayton F, Kulkarni V, Alicea C, Rosati M, Chowdhury B, Gautam R, Broderick KE, Sardesai NY, Martin MA, Mullins JI, Pavlakis GN, Felber BK.** 2016. DNA Prime-Boost Vaccine Regimen To Increase Breadth, Magnitude, and Cytotoxicity of the Cellular Immune Responses to Subdominant Gag Epitopes of Simian Immunodeficiency Virus and HIV. J Immunol **197:**3999-4013.
43. **Hu X, Valentin A, Rosati M, Manocheewa S, Alicea C, Chowdhury B, Bear J, Broderick KE, Sardesai NY, Gall SL, Mullins JI, Pavlakis GN, Felber BK.** 2017. HIV Env conserved element DNA vaccine alters immunodominance in macaques. Hum Vaccin Immunother **13:**2859-2871.
44. **Ake JA, Schuetz A, Pegu P, Wieczorek L, Eller MA, Kibuuka H, Sawe F, Maboko L, Polonis V, Karasavva N, Weiner D, Sekiziyivu A, Kosgei J, Missanga M, Kroidl A, Mann P, Ratto-Kim S, Anne Eller L, Earl P, Moss B, Dorsey-Spitz J, Milazzo M, Laissa Ouedraogo G, Rizvi F, Yan J, Khan AS, Peel S, Sardesai NY, Michael NL, Ngauy V, Marovich M, Robb ML.** 2017. Safety and Immunogenicity of PENNVAX-G DNA Prime Administered by Biojector 2000 or CELLECTRA Electroporation Device With Modified Vaccinia Ankara-CMDR Boost. J Infect Dis **216:**1080-1090.
45. **Kalams SA, Parker SD, Elizaga M, Metch B, Edupuganti S, Hural J, De Rosa S, Carter DK, Rybczyk K, Frank I, Fuchs J, Koblin B, Kim DH, Joseph P, Keefer MC, Baden LR, Eldridge J, Boyer J, Sherwat A, Cardinali M, Allen M, Pensiero M, Butler C, Khan AS, Yan J, Sardesai NY, Kublin JG, Weiner DB, Network NHVT.** 2013. Safety and comparative immunogenicity of an HIV-1 DNA vaccine in combination with plasmid interleukin 12 and impact of intramuscular electroporation for delivery. J Infect Dis **208:**818-829.
46. **Vaccari M, Gordon SN, Fourati S, Schifanella L, Liyanage NP, Cameron M, Keele BF, Shen X, Tomaras GD, Billings E, Rao M, Chung AW, Dowell KG, Bailey-Kellogg C, Brown EP, Ackerman ME, Vargas-Inchaustegui DA, Whitney S, Doster MN, Binello N, Pegu P, Montefiori DC, Foulds K, Quinn DS, Donaldson M, Liang F, Lore K, Roederer M, Koup RA, McDermott A, Ma ZM, Miller CJ, Phan TB, Forthal DN, Blackburn M, Caccuri F, Bissa M, Ferrari G, Kalyanaraman V, Ferrari MG, Thompson D, Robert-Guroff M, Ratto-Kim S, Kim JH, Michael NL, Phogat S, Barnett SW, Tartaglia J, Venzon D, Stablein DM, et al.** 2016. Adjuvant-dependent innate and adaptive immune signatures of risk of SIVmac251 acquisition. Nat Med **22:**762-770.
47. **Hill DL, Pierson W, Bolland DJ, Mkindi C, Carr EJ, Wang J, Houard S, Wingett SW, Audran R, Wallin EF, Jongo SA, Kamaka K, Zand M, Spertini F, Daubenberger C, Corcoran AE, Linterman MA.** 2019. The adjuvant GLA-SE promotes human Tfh cell expansion and emergence of public TCRbeta clonotypes. J Exp Med doi:10.1084/jem.20190301.

48. **van Diepen MT, Chapman R, Moore PL, Margolin E, Hermanus T, Morris L, Ximba P, Rybicki EP, Williamson AL.** 2018. The adjuvant AlhydroGel elicits higher antibody titres than AddaVax when combined with HIV-1 subtype C gp140 from CAP256. PLoS One **13:**e0208310.
49. **Kang TH, Bae HC, Kim SH, Seo SH, Son SW, Choi EY, Seong SY, Kim TW.** 2009. Modification of dendritic cells with interferon-gamma-inducible protein-10 gene to enhance vaccine potency. J Gene Med **11:**889-898.
50. **Xu W, Joo H, Clayton S, Dullaers M, Herve MC, Blankenship D, De La Morena MT, Balderas R, Picard C, Casanova JL, Pascual V, Oh S, Banchereau J.** 2012. Macrophages induce differentiation of plasma cells through CXCL10/IP-10. J Exp Med **209:**1813-1823, S1811-1812.
51. **Singh S, Ramirez-Salazar EG, Doueiri R, Valentin A, Rosati M, Hu X, Keele BF, Shen X, Tomaras GD, Ferrari G, LaBranche C, Montefiori DC, Das J, Alter G, Trinh HV, Hamlin C, Rao M, Dayton F, Bear J, Chowdhury B, Alicea C, Lifson JD, Broderick KE, Sardesai NY, Sivananthan SJ, Fox CB, Reed SG, Venzon DJ, Hirsch VM, Pavlakis GN, Felber BK.** 2018. Control of Heterologous Simian Immunodeficiency Virus SIVsmE660 Infection by DNA and Protein Coimmunization Regimens Combined with Different Toll-Like-Receptor-4-Based Adjuvants in Macaques. J Virol **92**.
52. **Iyer SS, Latner DR, Zilliox MJ, McCausland M, Akondy RS, Penaloza-Macmaster P, Hale JS, Ye L, Mohammed AU, Yamaguchi T, Sakaguchi S, Amara RR, Ahmed R.** 2013. Identification of novel markers for mouse CD4(+) T follicular helper cells. Eur J Immunol **43:**3219-3232.
53. **Carnathan DG, Wetzel KS, Yu J, Lee ST, Johnson BA, Paiardini M, Yan J, Morrow MP, Sardesai NY, Weiner DB, Ertl HC, Silvestri G.** 2014. Activated CD4+CCR5+ T cells in the rectum predict increased SIV acquisition in SIVGag/Tat-vaccinated rhesus macaques. Proc Natl Acad Sci U S A doi:10.1073/pnas.1407466112.
54. **Stieh DJ, Matias E, Xu H, Fought AJ, Blanchard JL, Marx PA, Veazey RS, Hope TJ.** 2016. Th17 Cells Are Preferentially Infected Very Early after Vaginal Transmission of SIV in Macaques. Cell Host Microbe **19:**529-540.
55. **Crescioli S, Correa I, Karagiannis P, Davies AM, Sutton BJ, Nestle FO, Karagiannis SN.** 2016. IgG4 Characteristics and Functions in Cancer Immunity. Curr Allergy Asthma Rep **16:**7.
56. **Boesch AW, Osei-Owusu NY, Crowley AR, Chu TH, Chan YN, Weiner JA, Bharadwaj P, Hards R, Adamo ME, Gerber SA, Cocklin SL, Schmitz JE, Miles AR, Eckman JW, Belli AJ, Reimann KA, Ackerman ME.** 2016. Biophysical and Functional Characterization of Rhesus Macaque IgG Subclasses. Front Immunol **7:**589.
57. **Gorse GJ, Corey L, Patel GB, Mandava M, Hsieh RH, Matthews TJ, Walker MC, McElrath MJ, Berman PW, Eibl MM, Belshe RB.** 1999. HIV-1MN recombinant glycoprotein 160 vaccine-induced cellular and humoral immunity boosted by HIV-1MN recombinant glycoprotein 120 vaccine. National Institute of Allergy and Infectious Diseases AIDS Vaccine Evaluation Group. AIDS Res Hum Retroviruses **15:**115-132.
58. **Chan YN, Boesch AW, Osei-Owusu NY, Emileh A, Crowley AR, Cocklin SL, Finstad SL, Linde CH, Howell RA, Zentner I, Cocklin S, Miles AR, Eckman JW, Alter G, Schmitz JE, Ackerman ME.** 2016. IgG Binding Characteristics of Rhesus Macaque FcgammaR. J Immunol **197:**2936-2947.
59. **Warncke M, Calzascia T, Coulot M, Balke N, Touil R, Kolbinger F, Heusser C.** 2012. Different adaptations of IgG effector function in human and nonhuman primates and implications for therapeutic antibody treatment. J Immunol **188:**4405-4411.
60. **Christensen D, Mortensen R, Rosenkrands I, Dietrich J, Andersen P.** 2017. Vaccine-induced Th17 cells are established as resident memory cells in the lung and promote local IgA responses. Mucosal Immunol **10:**260-270.
61. **Lycke NY, Bemark M.** 2017. The regulation of gut mucosal IgA B-cell responses: recent developments. Mucosal Immunol **10:**1361-1374.
62. **Ramakrishnan A, Schumack NM, Gariepy CL, Eggleston H, Nunez G, Espinoza N, Nieto M, Castillo R, Rojas J, McCoy AJ, Beck Z, Matyas GR, Alving CR, Guerry P, Poly F, Laird RM.** 2019. Enhanced Immunogenicity and Protective Efficacy of a Campylobacter jejuni Conjugate Vaccine Coadministered with Liposomes Containing Monophosphoryl Lipid A and QS-21. mSphere **4**.
63. **Mulligan MJ, Russell ND, Celum C, Kahn J, Noonan E, Montefiori DC, Ferrari G, Weinhold KJ, Smith JM, Amara RR, Robinson HL, Network NNDHVT.** 2006. Excellent safety and tolerability of the human immunodeficiency virus type 1 pGA2/JS2 plasmid DNA priming vector vaccine in HIV type 1 uninfected adults. AIDS Res Hum Retroviruses **22:**678-683.

64. **Styles TM, Gangadhara S, Reddy PBJ, Hicks S, LaBranche C C, Montefiori DC, Derdeyn CA, Kozlowski PA, Velu V, Amara RR.** HIV C.1086 Envelope Gp140 Protein Boosts Following DNA/MVA Vaccination 1
Fail to Enhance Heterologous Anti-V1V2 Antibody Response and Protection 2 Against Clade C SHIV Challenge.

65. **Xu Y, Fernandez C, Alcantara S, Bailey M, De Rose R, Kelleher AD, Zaunders J, Kent SJ.** 2013. Serial study of lymph node cell subsets using fine needle aspiration in pigtail macaques. J Immunol Methods **394:**73-83.

66. **Kozlowski PA, Lynch RM, Patterson RR, Cu-Uvin S, Flanigan TP, Neutra MR.** 2000. Modified wick method using Weck-Cel sponges for collection of human rectal secretions and analysis of mucosal HIV antibody. J Acquir Immune Defic Syndr **24:**297-309.

67. **Pegu P, Vaccari M, Gordon S, Keele BF, Doster M, Guan Y, Ferrari G, Pal R, Ferrari MG, Whitney S, Hudacik L, Billings E, Rao M, Montefiori D, Tomaras G, Alam SM, Fenizia C, Lifson JD, Stablein D, Tartaglia J, Michael N, Kim J, Venzon D, Franchini G.** 2013. Antibodies with high avidity to the gp120 envelope protein in protection from simian immunodeficiency virus SIV(mac251) acquisition in an immunization regimen that mimics the RV-144 Thai trial. J Virol **87:**1708-1719.

68. **Tomaras GD, Binley JM, Gray ES, Crooks ET, Osawa K, Moore PL, Tumba N, Tong T, Shen X, Yates NL, Decker J, Wibmer CK, Gao F, Alam SM, Easterbrook P, Abdool Karim S, Kamanga G, Crump JA, Cohen M, Shaw GM, Mascola JR, Haynes BF, Montefiori DC, Morris L.** 2011. Polyclonal B cell responses to conserved neutralization epitopes in a subset of HIV-1-infected individuals. J Virol **85:**11502-11519.

69. **Iyer SS, Gangadhara S, Victor B, Shen X, Chen X, Nabi R, Kasturi SP, Sabula MJ, Labranche CC, Reddy PB, Tomaras GD, Montefiori DC, Moss B, Spearman P, Pulendran B, Kozlowski PA, Amara RR.** 2016. Virus-Like Particles Displaying Trimeric Simian Immunodeficiency Virus (SIV) Envelope gp160 Enhance the Breadth of DNA/Modified Vaccinia Virus Ankara SIV Vaccine-Induced Antibody Responses in Rhesus Macaques. J Virol **90:**8842-8854.

70. **Alpert MD, Heyer LN, Williams DE, Harvey JD, Greenough T, Allhorn M, Evans DT.** 2012. A novel assay for antibody-dependent cell-mediated cytotoxicity against HIV-1- or SIV-infected cells reveals incomplete overlap with antibodies measured by neutralization and binding assays. J Virol **86:**12039-12052.

71. **von Bredow B, Arias JF, Heyer LN, Gardner MR, Farzan M, Rakasz EG, Evans DT.** 2015. Envelope Glycoprotein Internalization Protects Human and Simian Immunodeficiency Virus-Infected Cells from Antibody-Dependent Cell-Mediated Cytotoxicity. J Virol **89:**10648-10655.

72. **Phillips B, Fouda GG, Eudailey J, Pollara J, Curtis AD, 2nd, Kunz E, Dennis M, Shen X, Bay C, Hudgens M, Pickup D, Alam SM, Ardeshir A, Kozlowski PA, Van Rompay KKA, Ferrari G, Moody MA, Permar S, De Paris K.** 2017. Impact of Poxvirus Vector Priming, Protein Coadministration, and Vaccine Intervals on HIV gp120 Vaccine-Elicited Antibody Magnitude and Function in Infant Macaques. Clin Vaccine Immunol **24**.

73. **Petitdemange C, Kasturi SP, Kozlowski PA, Nabi R, Quarnstrom CF, Reddy PBJ, Derdeyn CA, Spicer LM, Patel P, Legere T, Kovalenkov YO, Labranche CC, Villinger F, Tomai M, Vasilakos J, Haynes B, Kang CY, Gibbs JS, Yewdell JW, Barouch D, Wrammert J, Montefiori D, Hunter E, Amara RR, Masopust D, Pulendran B.** 2019. Vaccine induction of antibodies and tissue-resident CD8+ T cells enhances protection against mucosal SHIV-infection in young macaques. JCI Insight **4**.

74. **Manrique M, Kozlowski PA, Cobo-Molinos A, Wang SW, Wilson RL, Montefiori DC, Mansfield KG, Carville A, Aldovini A.** 2011. Long-term control of simian immunodeficiency virus mac251 viremia to undetectable levels in half of infected female rhesus macaques nasally vaccinated with simian immunodeficiency virus DNA/recombinant modified vaccinia virus Ankara. J Immunol **186:**3581-3593.

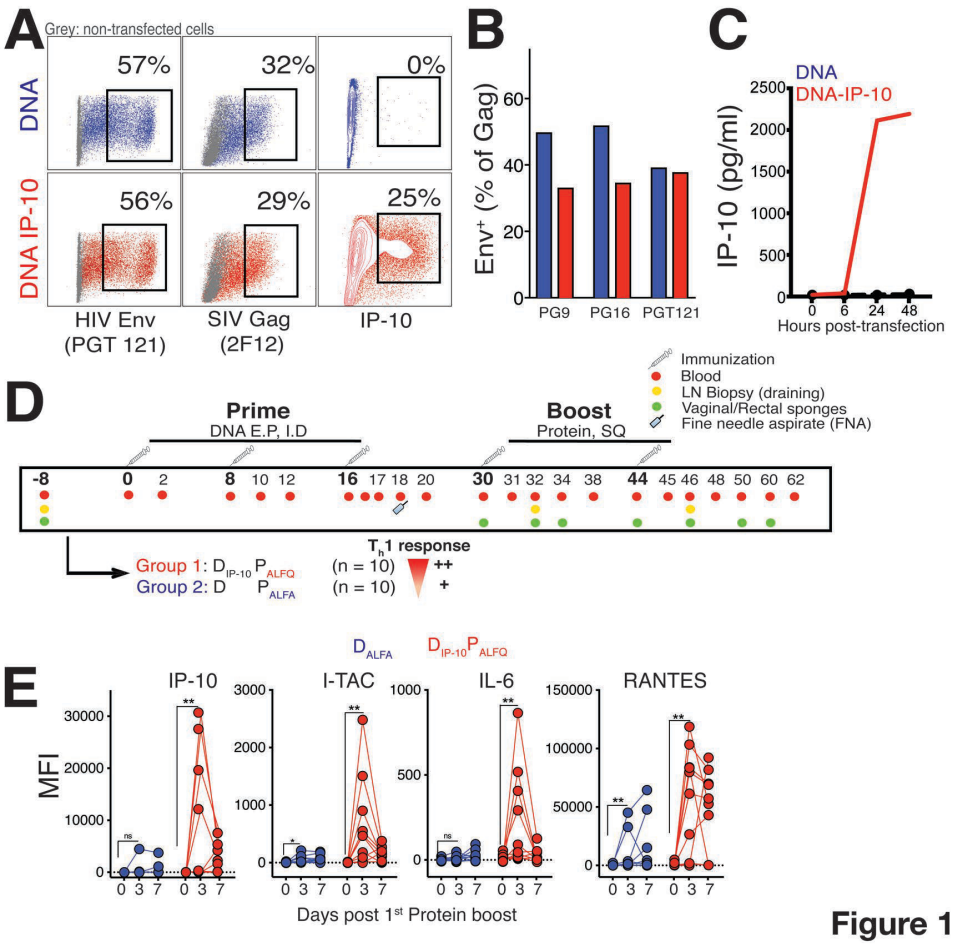

Figure 1

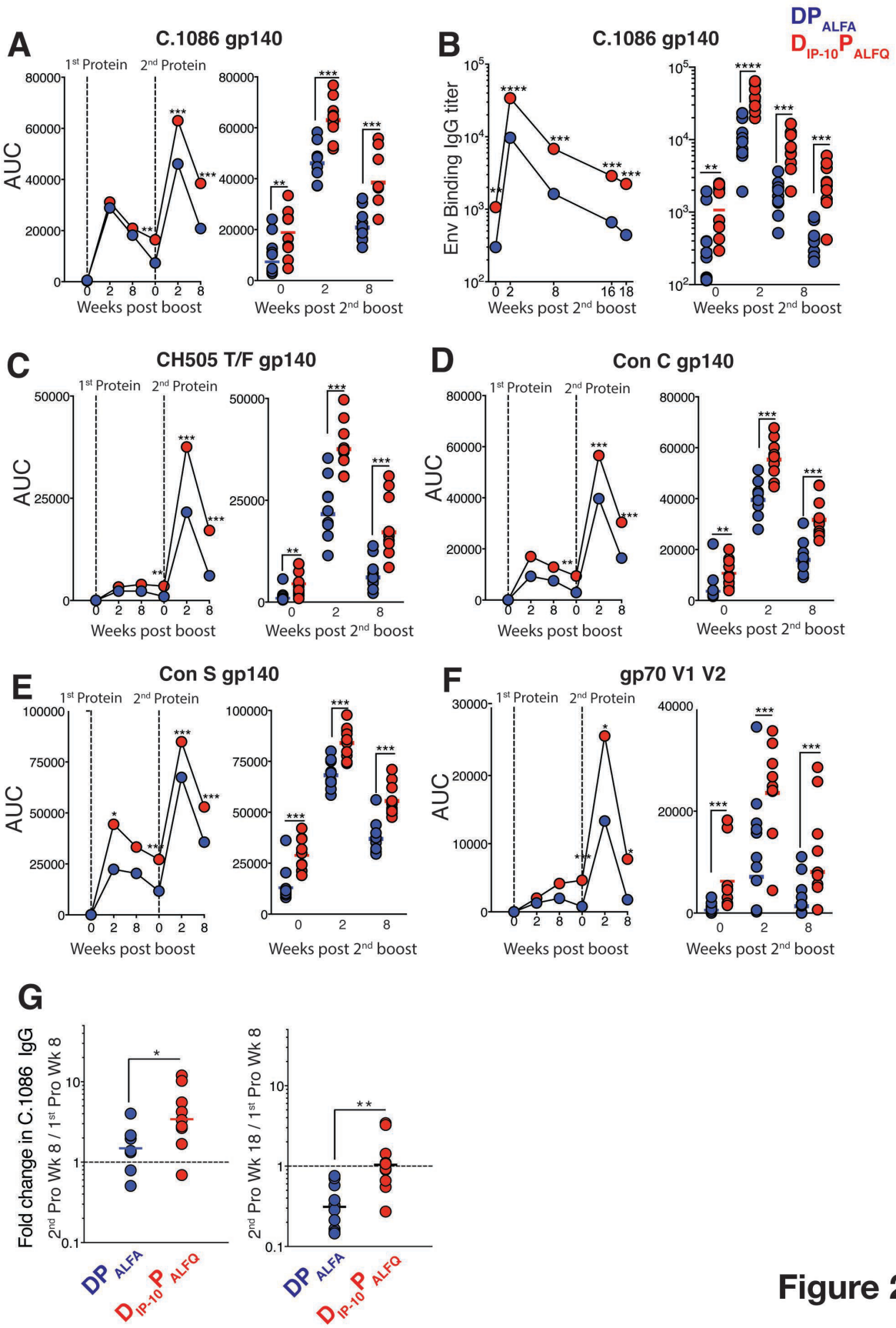

Figure 2

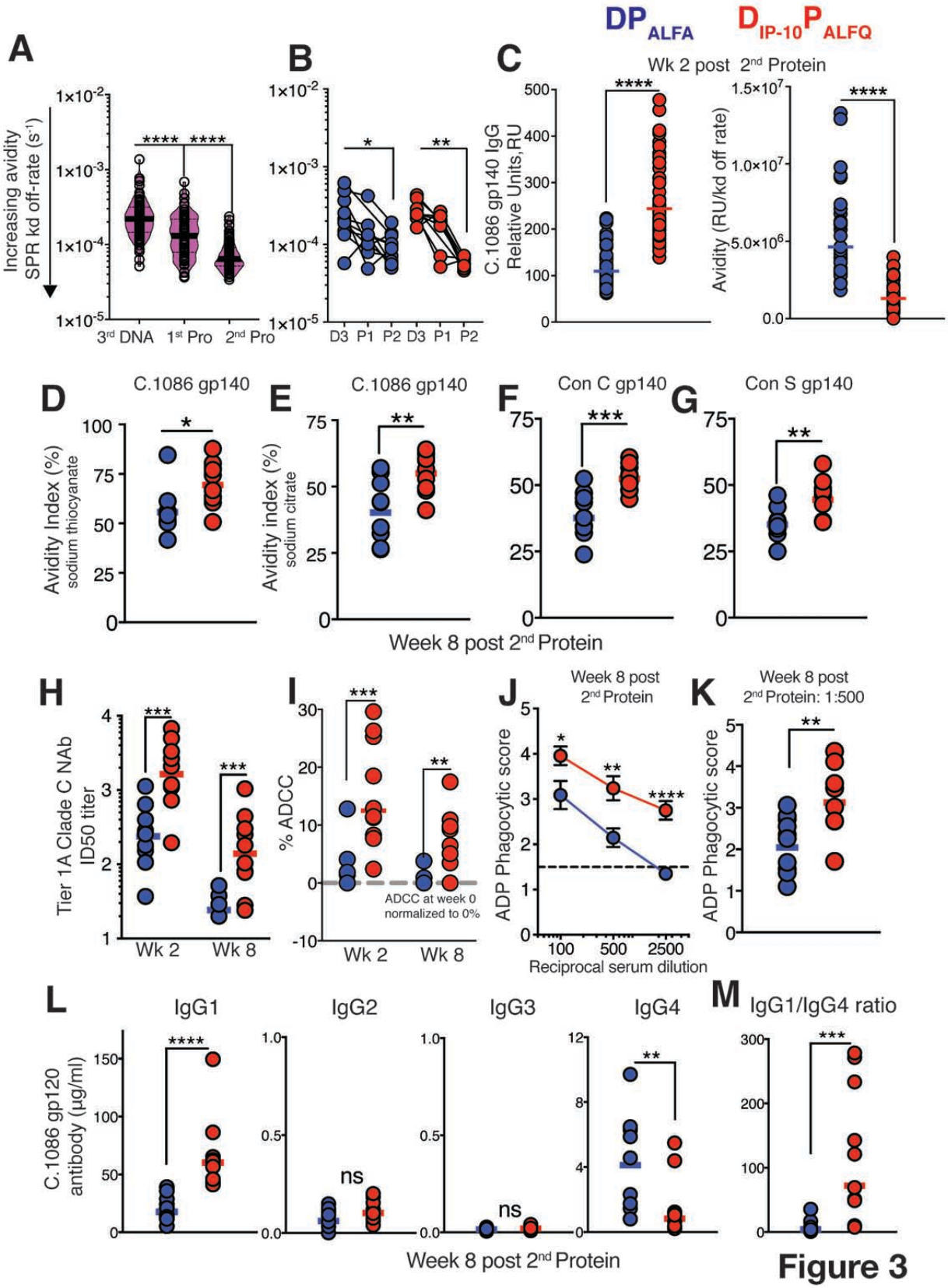

Figure 3

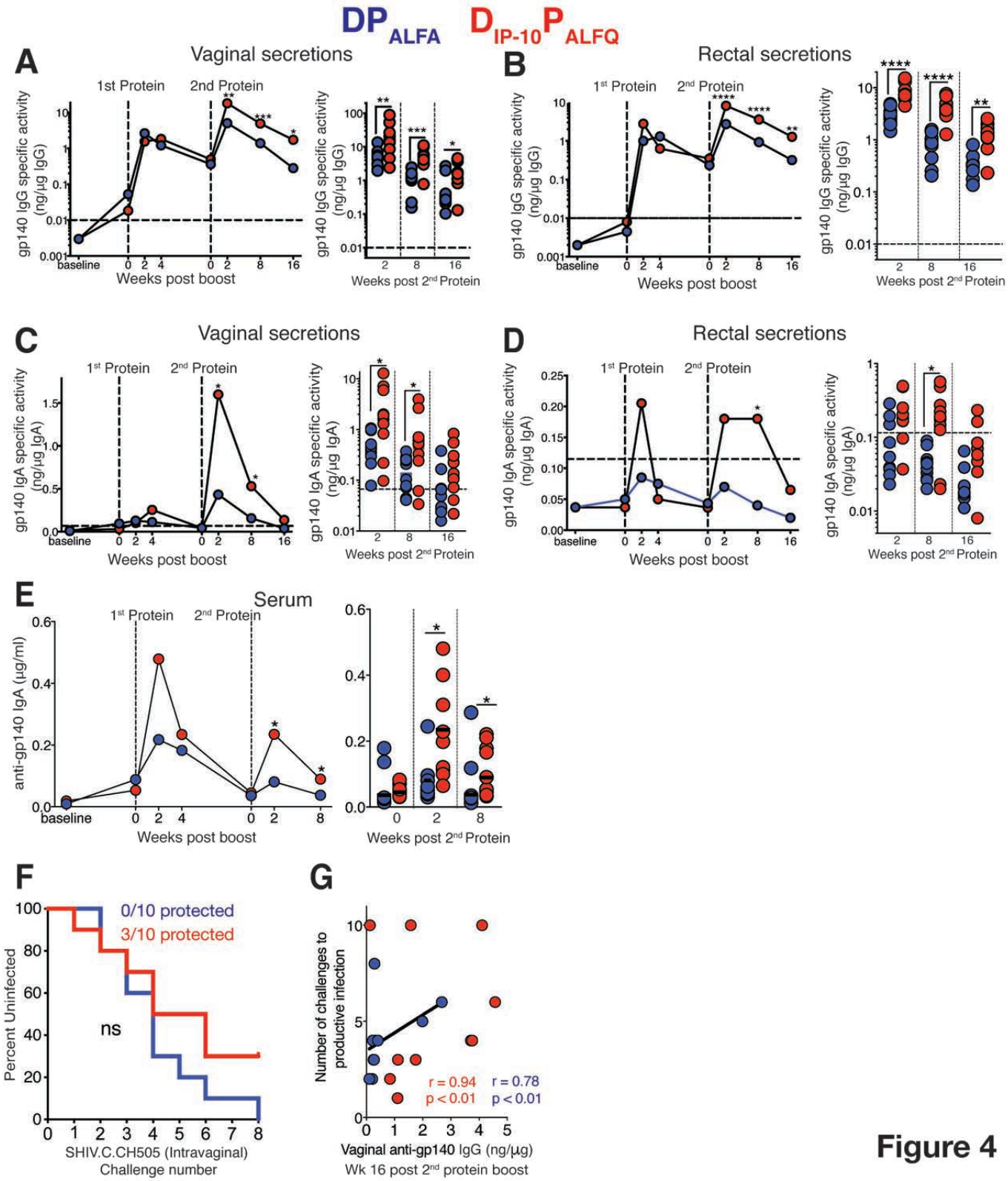

Figure 4

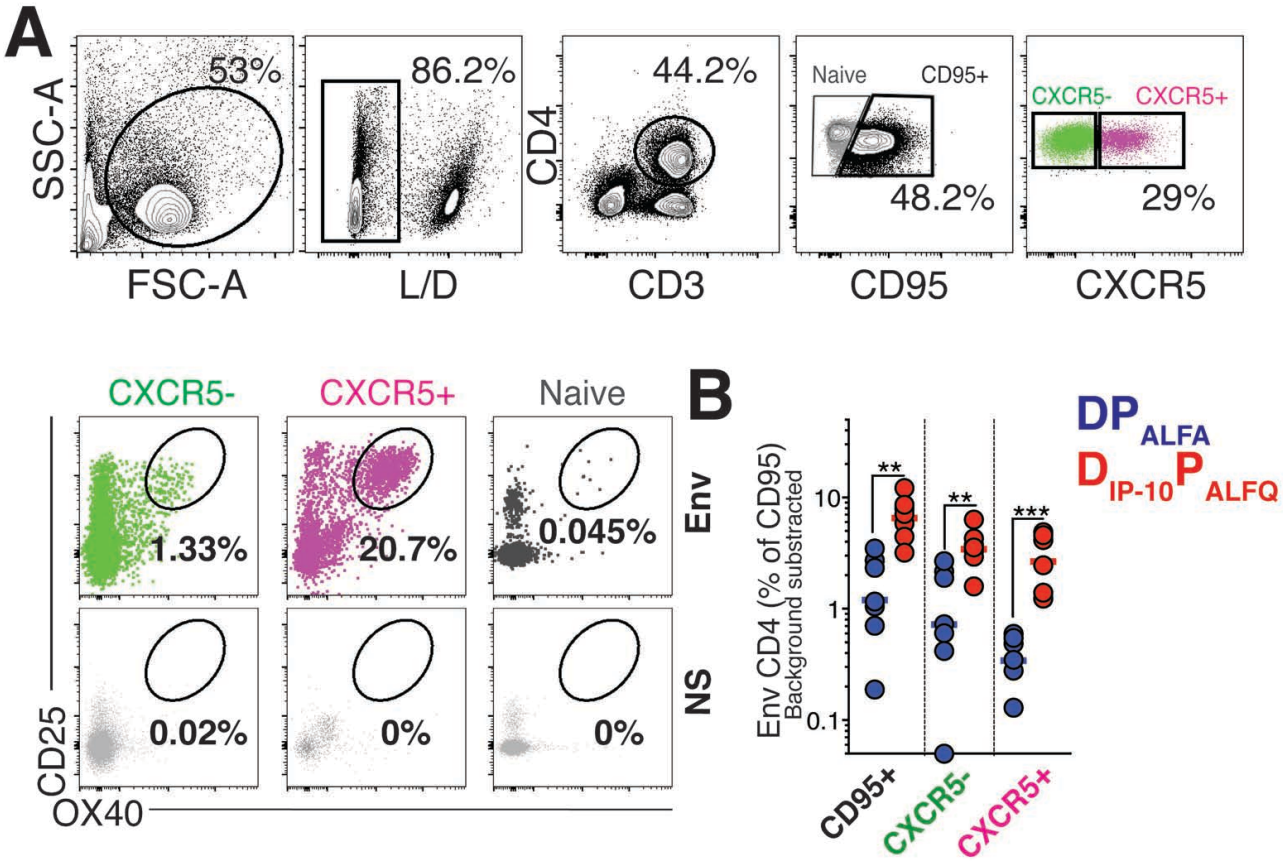

Figure 5

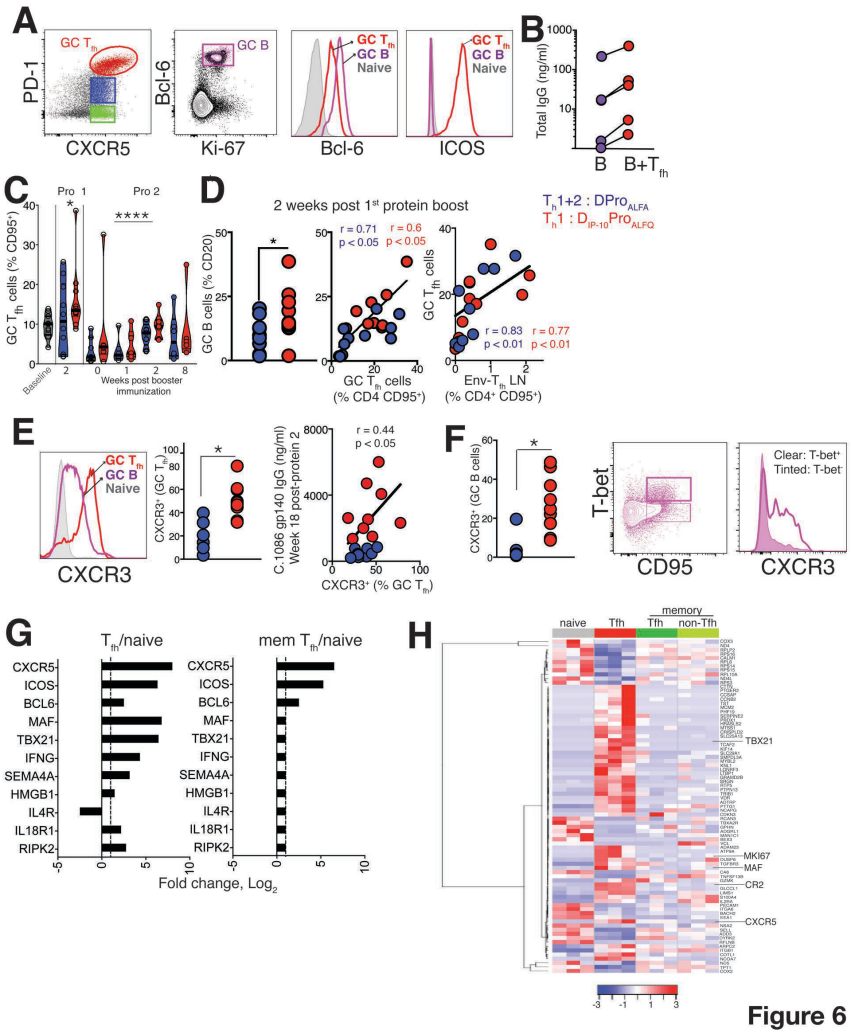

Figure 6

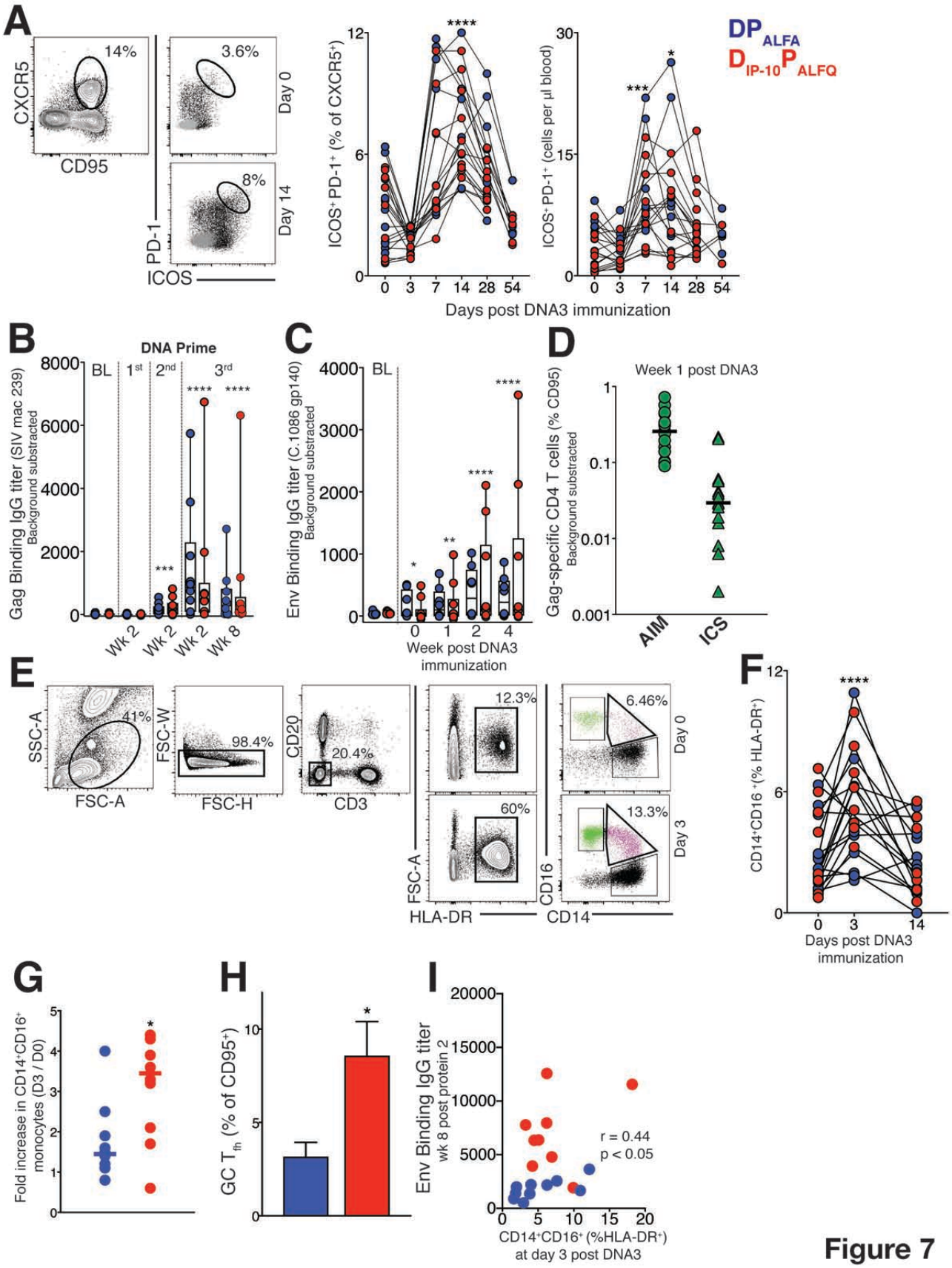

Figure 7